

RNF186 regulates EFNB1 (ephrin B1)-EPHB2-induced autophagy in the colonic epithelial cells for the maintenance of intestinal homeostasis

Huazhi Zhang , Zhihui Cui , Du Cheng , Yanyun Du , Xiaoli Guo , Ru Gao , Jianwen Chen , Wanwei Sun , Ruirui He , Xiaojian Ma , Qianwen Peng , Bradley N. Martin , Wei Yan , Yueguang Rong & Chenhui Wang

To cite this article: Huazhi Zhang , Zhihui Cui , Du Cheng , Yanyun Du , Xiaoli Guo , Ru Gao , Jianwen Chen , Wanwei Sun , Ruirui He , Xiaojian Ma , Qianwen Peng , Bradley N. Martin , Wei Yan , Yueguang Rong & Chenhui Wang (2020): RNF186 regulates EFNB1 (ephrin B1)-EPHB2-induced autophagy in the colonic epithelial cells for the maintenance of intestinal homeostasis, *Autophagy*, DOI: [10.1080/15548627.2020.1851496](https://doi.org/10.1080/15548627.2020.1851496)

To link to this article: <https://doi.org/10.1080/15548627.2020.1851496>



[View supplementary material](#)



Published online: 17 Dec 2020.



[Submit your article to this journal](#)



Article views: 248



[View related articles](#)




[View Crossmark data](#)

RESEARCH PAPER



RNF186 regulates EFNB1 (ephrin B1)-EPHB2-induced autophagy in the colonic epithelial cells for the maintenance of intestinal homeostasis

Huazhi Zhang^{a,*}, Zhihui Cui^{a,*}, Du Cheng^b, Yanyun Du^a, Xiaoli Guo^a, Ru Gao^a, Jianwen Chen^a, Wanwei Sun^a, Ruirui He^a, Xiaojian Ma^a, Qianwen Peng^a, Bradley N. Martin^c, Wei Yan^d, Yueguang Rong^e, and Chenhui Wang^g

^aKey Laboratory of Molecular Biophysics of the Ministry of Education, National Engineering Research Center for Nanomedicine, College of Life Science and Technology, Huazhong University of Science and Technology, Wuhan, China; ^bDepartment of Gastroenterology, Renmin Hospital of Wuhan University, Wuhan, China; ^cDepartment of Medicine, Brigham and Women's Hospital, Harvard Medical School, Boston, MA, USA; ^dDepartment of Gastroenterology, Tongji Hospital, Tongji Medical College, Huazhong University of Science and Technology Wuhan, China; ^eDepartment of Pathogen Biology, School of Basic Medicine, Huazhong University of Science and Technology, Wuhan, China; ^fDepartment of Bioinformatics, Wuhan Institute of Biotechnology, Wuhan, China

ABSTRACT

Although genome-wide association studies have identified the gene *RNF186* encoding an E3 ubiquitin-protein ligase as conferring susceptibility to ulcerative colitis, the exact function of this protein remains unclear. In the present study, we demonstrate an important role for RNF186 in macroautophagy/autophagy activation in colonic epithelial cells and intestinal homeostasis. Mechanistically, RNF186 acts as an E3 ubiquitin-protein ligase for EPHB2 and regulates the ubiquitination of EPHB2. Upon stimulation by ligand EFNB1 (ephrin B1), EPHB2 is ubiquitinated by RNF186 at Lys892, and further recruits MAP1LC3B for autophagy. Compared to control mice, *rnf186*^{-/-} and *ephb2*^{-/-} mice have a more severe phenotype in the DSS-induced colitis model, which is due to a defect in autophagy in colon epithelial cells. More importantly, treatment with ephrin-B1-Fc recombinant protein effectively relieves DSS-induced mouse colitis, which suggests that ephrin-B1-Fc may be a potential therapy for human inflammatory bowel diseases.

Abbreviations: ACTB: actin beta; ATG5: autophagy related 5; ATG16L1: autophagy related 16 like 1; ATP: adenosine triphosphate; Cas9: CRISPR associated protein 9; CD: Crohn disease; CQ: chloroquine; *Csf2*: colony stimulating factor 2; *Cxcl1*: c-x-c motif chemokine ligand 1; DMSO: dimethyl sulfoxide; DSS: dextran sodium sulfate; EFNB1: ephrin B1; EPHB2: EPH receptor B2; EPHB3: EPH receptor B3; EPHB2^{K788R}: lysine 788 mutated to arginine in EPHB2; EPHB2^{K892R}: lysine 892 mutated to arginine in EPHB2; ER: endoplasmic reticulum; FITC: fluorescein isothiocyanate; GFP: green fluorescent protein; GWAS: genome-wide association studies; HRP: horseradish peroxidase; HSPA5/BiP: heat shock protein family A (Hsp70) member 5; IBD: inflammatory bowel diseases; *Il1b*: interleukin 1 beta; *Il6*: interleukin 6; IRGM: immunity related GTPase M; i.p.: intraperitoneally; IPP: inorganic pyrophosphatase; KD: knock-down; KO: knockout; MAP1LC3B: microtubule associated protein 1 light chain 3 beta; MTOR: mechanistic target of rapamycin kinase; NOD2: nucleotide binding oligomerization domain containing 2; PI3K: phosphoinositide 3-kinase; PtdIns3K: class III phosphatidylinositol 3-kinase; RNF186: ring finger protein 186; RNF186^{A64T}: alanine 64 mutated to threonine in RNF186; RNF186^{R179X}: arginine 179 mutated to X in RNF186; RPS6: ribosomal protein S6; *Tnf*: tumor necrosis factor; SQSTM1: sequestosome 1; Ub: ubiquitin; UBE2D2: ubiquitin conjugating enzyme E2 D2; UBE2H: ubiquitin conjugating enzyme E2 H; UBE2K: ubiquitin conjugating enzyme E2 K; UBE2N: ubiquitin conjugating enzyme E2 N; UC: ulcerative colitis; ULK1:unc-51 like autophagy activating kinase 1; WT: wild type.

ARTICLE HISTORY

Received 9 December 2019
Revised 8 November 2020
Accepted 11 November 2020





KEYWORDS

Autophagy; EPHB2; ephrin B1; RNF186; ulcerative colitis


Introduction

Inflammatory bowel diseases (IBD), which include Crohn disease (CD) and ulcerative colitis (UC), are characterized by chronic and recurrent inflammation of the gastrointestinal tract despite exhibiting distinct pathophysiological features. UC induces a continuous pattern of inflammation that involves the superficial mucosal and submucosal layers and

is limited to the colon. Conversely, CD is associated with discontinuous areas of inflammation, which may affect any region of the gut [1,2]. Although the precise pathology of IBD remains uncertain, accumulating evidence suggests that multiple genetic, environmental, and immunological factors contribute to disease initiation and progression [3–5]. Patients with a long history of UC or CD face an increased risk of

CONTACT Yueguang Rong  rongyueguang@hust.edu.cn  Department of Pathogen Biology, School of Basic Medicine, Huazhong University of Science and Technology, Wuhan, China; Chenhui Wang  wangchenhui@hust.edu.cn  Key Laboratory of Molecular Biophysics of the Ministry of Education, National Engineering Research Center for Nanomedicine, College of Life Science and Technology, Huazhong University of Science and Technology, 1037th Luoyu Ave., Wuhan 430074, China

*These authors contribute equally to this work

 Supplemental data for this article can be accessed [here](#).

© 2020 Informa UK Limited, trading as Taylor & Francis Group

developing colorectal cancer, while those with small intestinal CD also face an increased risk of developing small bowel adenocarcinoma [6,7].

Autophagy is a highly evolutionarily-conserved process of cellular self-digestion. This process involves the sequestration of excessive, damaged, or aged proteins and intracellular pathogens in double-membranous vesicles called “autophagosomes,” which then fuse with lysosomes to form “autolysosomes.” Autophagy plays an important role in the regulation of multiple cellular processes, including cell development, differentiation, survival, and senescence [8–10]. The autophagic machinery is used in immune defense against microbes, including the specific targeting and delivery of microorganisms to degradation in the lysosome (a process referred to as xenophagy) [8]. The xenophagy machinery dysregulation will cause susceptibility to IBD. To date, genome-wide association studies (GWAS) have identified several genes associated with IBD susceptibility. Several of these genes encode proteins considered relevant to autophagy, including *Atg16l1* (autophagy related 16 like 1) [11,12], *ULK1* (unc-51 like autophagy activating kinase 1) [13], *IRGM* (immunity related GTPase M) [14,15] and *NOD2* (nucleotide binding oligomerization domain containing 2) [16]. Collectively, these findings suggest that autophagy plays an essential role in the host defense against intracellular pathogens and maintenance of intestinal homeostasis. However, the detailed molecular and cellular mechanisms of different genes conferring IBD susceptibility remain unclear.

EPH receptors comprise the largest subgroup of tyrosine kinase receptors and can be further subdivided into EPHA and EPHB receptors according to ligand-binding specificity (i.e., binding to A-type and B-type EFNs [ephrins], respectively) [17,18]. The EFN-EPH interaction activates bidirectional cell-cell communication between both the receptor-expressing (i.e., forward signaling) and ligand-expressing (i.e., reverse signaling) cells. However, these interactions involve direct cell-to-cell contact and frequently result in repulsion. To date, the roles of EPH receptor and EFNB signaling are best understood in the context of cell migration control and axon guidance. Recent studies have also identified this signaling axis as a regulator of progenitor cell proliferation [19–22]. In particular, EPHB receptors were found to regulate both cell migration and progenitor cell proliferation in the intestinal cells [23]. In addition, the observed association of losses of EPHB2 (EPH receptor B2) and EPHB3 (EPH receptor B3) expression with colorectal tumorigenesis and the detection of *EPHB2* mutations in clinical prostate cancer samples have led to the broad acceptance of these receptors as tumor suppressors [24–28]. However, the potential role of the EFNB-EPHB signaling axis in autoimmune diseases (e.g., IBD) remains uncertain.

Previous GWAS studies indicated that *RNF186* (ring finger protein 186), encoding a ring-finger domain-containing E3 ubiquitin-protein ligase, was associated with UC susceptibility [29–31]. In the previous study, two rare single nucleotide polymorphisms (SNPs) of *RNF186* were found to alter the amino acid sequence: *RNF186*^{A64T} and *RNF186*^{R179X}. Interestingly, individuals who carried the *RNF186*^{A64T} variant were susceptible to UC, whereas carriers of the *RNF186*^{R179X} variant were protected from UC, while the mechanism of these two variants which leads to distinct UC susceptibility

was unclear [29,31]. A recent study found that *RNF186* maintains gut homeostasis by controlling ER stress in colonic epithelia, but the detailed mechanism is still unclear, including the substrate(s) of *RNF186* in the epithelial cells [32]. In this study, we identify a critical role of *RNF186* in the ligand protein EFNB-induced autophagy in colonic epithelial cells, as well as for the intracellular bacterial clearance. Through *in vivo* and *in vitro* mechanistic studies, we find that *RNF186* acts as an E3 ubiquitin-protein ligase for EPHB2, and regulates the ubiquitination of EPHB2 upon ligand protein EFNB1 stimulation. Through mass spectrometry identification and experimental analysis, it is found that Lys892 of EPHB2 is important to EPHB2-MAP1LC3B (microtubule associated protein 1 light chain 3 beta) binding and EFNB1-induced autophagy. Interestingly, a human UC susceptible mutant *RNF186*^{A64T}, loses the interaction with EPHB2 and has decreased E3 catalytic ability for EPHB2, whereas the UC protective mutant, *RNF186*^{R179X}, increases interaction with EPHB2. Finally, we investigate the effect of *Rnf186* and *Ephb2* deficiency in a dextran sodium sulfate (DSS)-induced mouse model of colitis and demonstrate the ability of ephrin-B1-Fc recombinant protein to relieve colitis symptoms by increasing autophagy in colonic epithelial cells. Overall, our study not only identifies a novel EFNB-induced autophagy through EPHB2 and *RNF186* in colonic epithelial cells, but also provides a potential treatment for human Inflammatory bowel diseases.

RESULTS

RNF186 is required for basal level of autophagy maintenance

To understand the relationship between *RNF186* and UC susceptibility, we first examined differences in *Rnf186* mRNA expression among different tissues in mice. Consistent with the gene expression database BioGPS (<http://biogps.org/#goto=genereport&id=54546>), *Rnf186* was mainly expressed in the colon and small intestine, although elevated expression levels were also observed in the kidney and liver (Figure 1A).

Next, we explored whether the knockdown (KD) or knock-out (KO) of *RNF186* would affect endoplasmic reticulum (ER) stress or autophagy level, as both mechanisms have been shown to play essential roles in the maintenance of intestinal homeostasis and the initiation and development of IBD. Moreover, a previous study found that *RNF186* could regulate ER stress [32,33]. In this study, we observed a considerable decrease in autophagy, as determined by decreased expression of the autophagosome marker MAP1LC3B-II and increased accumulation of SQSTM1 (sequestosome 1), in *RNF186* knockdown Ls174t human colonic cancer cell lines relative to control cells (Figure 1B). Specifically, compared to wild-type (WT) control cells, MAP1LC3B-II level was significantly decreased by 55.4% and SQSTM1 caused a roughly 2-fold increase in *RNF186* knockdown Ls174t cells (Figure 1B). By contrast, the expression of the ER stress marker *HSPA5*/BiP [heat shock protein family A (Hsp70) member 5] remained unaltered (Figure 1B). Next, we knocked out *RNF186* with

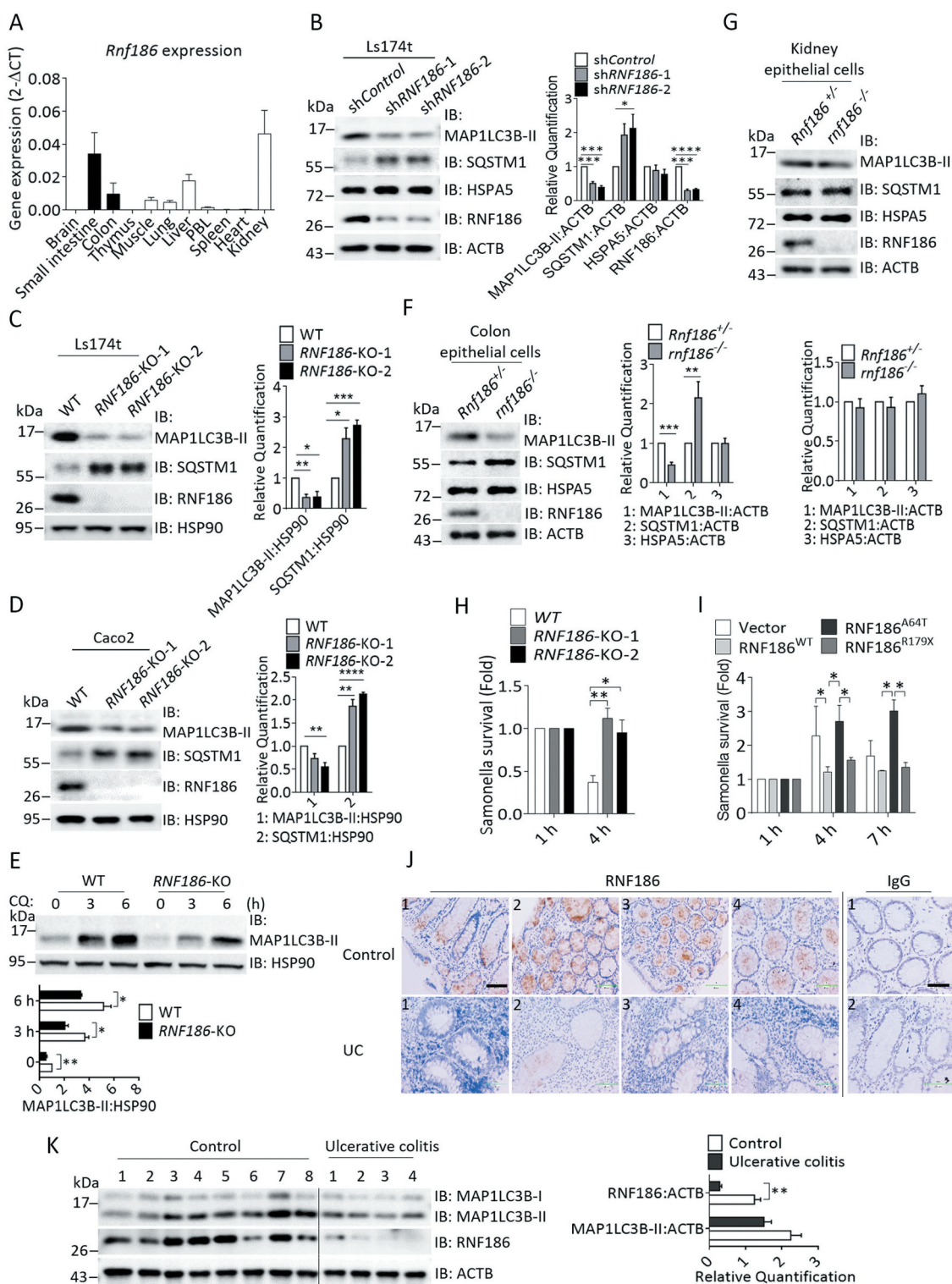


Figure 1. RNF186 is required for basal autophagy maintenance in colon epithelial cells. (A) qRT-PCR of *Rnf186* and *Actb* were done from different organs of three mice. (B and C) *RNF186* was knocked down (B) or knocked out (C) in Ls174t cells by shRNA and CRISPR-Cas9, followed by western blot analysis of the indicated proteins. Densitometry quantification from three independent experiments was shown in the right panel. (D) *RNF186* was knocked out in Caco2 cells by CRISPR-Cas9, followed by western blot analysis of the indicated proteins. Densitometry quantification from three independent experiments was shown in the right panel. (E) Control or *RNF186*-KO Caco2 cells were stimulated with DMSO or 50 μ M chloroquine (CQ) for the indicated time, followed by western blot analysis of the indicated proteins. Densitometry quantification from three independent experiments was shown in the bottom panel. (F and G) Mouse colonic epithelial cells (F) or kidney (G) epithelial cells from *Rnf186*^{-/-} mice or *rnf186*^{-/-} mice were harvested, followed by western blot analysis of the indicated proteins. Quantification were shown in the right panel and bottom panel. (H) Intracellular *Salmonella* number of control cells and two *RNF186*-KO cells were counted by serial dilution and plating after bacterial infection. (I) Intracellular *Salmonella* number of empty vectors, *RNF186*^{WT}, *RNF186*^{A64T} and *RNF186*^{R179X} stably transfected Ls174t cells was counted by serial dilution and plating after bacterial infection. (J) Immunohistochemistry staining of RNF186 from colonic biopsy samples of healthy control individuals or UC patients. Scale bar: 50 μ m. n = 4. (K) Western blot analysis of MAP1LC3B and RNF186 expression from colonic biopsy samples of healthy control individuals or ulcerative colitis patients was shown. Densitometry quantification was shown in the right panel. n = 8 and 4. WT: wild type; KO: knockout; UC: ulcerative colitis. All error bars represent SEM of technical replicates. *: P < 0.05, **: P < 0.01, ***: P < 0.001, ****: P < 0.0001 based on two-sided unpaired T test (B-I and K). Data are representative of three independent experiments.

CRISPR-Cas9 technique and examined autophagy in Ls174T and Caco2 cells respectively. We observed that MAP1LC3B-II level was significantly decreased by 64% and SQSTM1 increased by 2.5 fold in *RNF186* knockout Ls174t cells compared to WT control Ls174t cells (Figure 1C). In *RNF186* knockout Caco2 cells, MAP1LC3B-II level was significantly decreased by 36% and SQSTM1 increased by 2 fold compared with WT control cells (Figure 1D). We also confirmed that there was significantly reduced autophagosomes in *RNF186* knockout Ls174t cells compared to WT control Ls174t cells at basal condition by electron microscopy (Fig. S1).

To further investigate the role of RNF186 in autophagic flux, we treated *RNF186* knockout Caco2 cells with chloroquine (CQ), a lysosome inhibitor that result in the accumulation of MAP1LC3B-II by blocking the lysosomal degradation pathway. After blocking the autophagic flux by CQ, we observed a significant decrease in MAP1LC3B-II accumulation in *RNF186* knockout cells compared to the WT control cells, suggesting that RNF186 may be involved in a pathway which induces autophagy rather than accelerating the degradation of MAP1LC3B (Figure 1E). Consistent with the findings from human cell lines (Figure 1B-D), we also observed that in the colonic epithelial cells from *rnf186*^{-/-} mice, MAP1LC3B-II protein level was decreased by 55% and SQSTM1 protein level increased by 2.15 fold compared with that from *Rnf186*^{+/-} mice, while the HSPA5 level remained unchanged in these cells (Figure 1F). Interestingly, MAP1LC3B-II protein levels in kidney epithelial cells did not show any significant difference between *Rnf186*^{+/-} and *rnf186*^{-/-} mice, suggesting that the ability of RNF186 to regulate autophagy is tissue and cell-type specific (Figure 1G). Together, these data indicate that RNF186 plays a critical role in the maintenance of autophagy in the colonic epithelial cells.

Autophagy is required for the clearance of intracellular pathogens by intestinal epithelial cells. Therefore, we explored whether RNF186 deficiency affects the clearance of intracellular bacteria from colonic epithelial cells. Notably, we observed a significantly greater bacterial growth in *RNF186* knockout cells than that in control cells (Figure 1H), which was consistent with decreased levels of autophagy. As noted previously, RNF186^{A64T} confers susceptibility to UC. Interestingly, we observed a significantly slower rate of intracellular bacterial growth in cells overexpressing either RNF186 or RNF186^{R179X} (Figure 1I), while the overexpression of RNF186^{A64T} was associated with a relatively more rapid rate of bacterial growth compared with the control cells (Figure 1I), indicating that RNF186^{A64T} acts as a loss-of-function mutant in terms of intracellular bacterial clearance. In clinical samples, we observed strong RNF186 expression in human colorectal crypt epithelial cells from healthy individuals, but observed reduced expression in epithelial biopsy samples from UC patients (Figure 1J). Immunoblot analysis also indicated that the RNF186 protein level was decreased by 77% in the epithelial biopsy samples from UC patients compared to that from control individuals (Figure 1K). MAP1LC3B-II protein level was also reduced in the biopsy samples from UC patients compared to that from control individuals, while the difference did not reach significance, which may be due to the relatively small number of samples used in this experiment

(Figure 1K). These data suggest that RNF186 plays essential roles in the maintenance of basal autophagy and in intracellular bacterial clearance. Since the relationship between the dysregulation of autophagy and IBD susceptibility was well established by many prior studies, the susceptibility to UC conferred by *RNF186* polymorphisms may also be due to altered autophagy.

RNF186 ubiquitinates EPHB2 and EPHB3

Next, we performed immunoprecipitation and mass spectrometry identification to identify proteins that interacted with RNF186 in a human colonic cancer cell line Ls174t. Interestingly, EPHB2 and EPHB3 were identified as RNF186-interacting proteins (Figure 2A). We first confirmed the interaction of RNF186 with EPHB2 and EPHB3 by co-immunoprecipitation (Figure 2B). Next, we explored whether the mutants RNF186^{A64T} and RNF186^{R179X} could interact with EPHB2 and EPHB3. Interestingly, these two RNF186 mutants exhibited different patterns of EPH receptor binding. Specifically, RNF186^{A64T} lost the ability to interact with EPHB2 but could still bind to EPHB3 (Figure 2C, D). By contrast, the RNF186^{R179X} showed greater binding to EPHB2 but lost the ability to interact with EPHB3 (Figure 2C, D). EPHB2 was previously reported to be involved in autophagy [34] and the binding patterns of the RNF186 WT and mutant variants with EPHB2 were also consistent with our previous observations of intracellular bacterial clearance (Figure 1I) and with the susceptibility of *RNF186* polymorphisms to UC identified through human GWAS. Therefore, our subsequent experiments focused on the interaction between RNF186 and EPHB2.

Given that RNF186 has a RING finger domain, which has been shown to have E3 ubiquitin protein ligase activity, we examined the possibility that RNF186 acts as an E3 ligase for EPHB2 and EPHB3. We found that WT RNF186 ubiquitinated both EPHB2 and EPHB3, while the mutant RNF186^{A64T} exhibited a reduced ability to ubiquitinate EPHB2 but retained ability to ubiquitinate EPHB3, compared to WT RNF186 (Figure 2E, F). By contrast to RNF186^{A64T}, the RNF186^{R179X} exhibited a similar ability to ubiquitinate EPHB2 but was unable to ubiquitinate EPHB3 compared to the WT RNF186 (Figure 2E, F). These results were highly consistent with the observed interactions of RNF186 with EPHB2 and EPHB3 (Figure 2C-D). Polyubiquitination with linkage occurring at ubiquitin position K48 or K63 are the most frequent ubiquitin modifications, thus we examined whether the ubiquitin modifications of EPHB2 and EPHB3 by RNF186 were K48- or K63-linked, or neither. Utilizing Ubiquitin K48R or K63R mutants that cannot form K48- or K63-polyubiquitin chains, respectively, we found that EPHB2 ubiquitination by RNF186 was only modestly impacted (Figure 2G), while EPHB3 ubiquitination by RNF186 was markedly impaired compared to controls (Figure 2H). Using single-site reserved ubiquitin mutants, we found that RNF186 catalyzed multiple polyubiquitin linkage modifications on EPHB2, including ubiquitin-K27 (the primary target), -K29, -K33, -K48 and -K63 (Figure 2I). These results indicate that RNF186 mainly catalyzes K27-linked polyubiquitin chains on EPHB2, and K48- and K63-linked polyubiquitin chains on EPHB3. To further verify whether RNF186 is indeed an E3

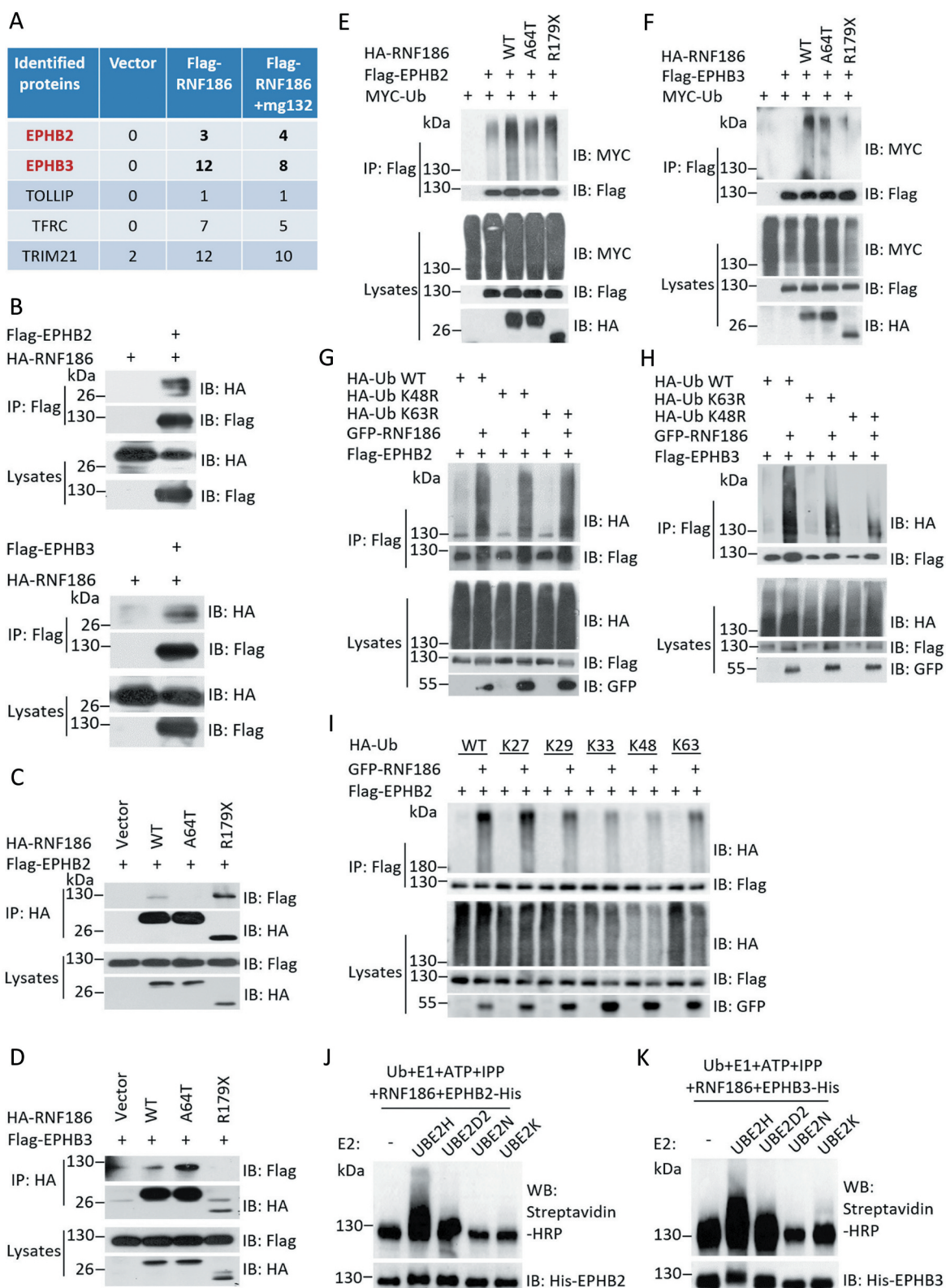


Figure 2. RNF186 binds to and ubiquitinates EPHB2 and EPHB3. (A) Indication of RNF186-interacting proteins identified by mass spectrometry. (B-D) 293 T cells were transfected as indicated, and cell lysates were immunoprecipitated by anti-Flag antibody (B) or anti-HA antibody (C and D), followed by western blot analysis of the indicated proteins. (E-I) 293 T cells were transfected as indicated, and cell lysates were immunoprecipitated by anti-Flag antibody, followed by western blot analysis of the indicated proteins. (J and K) *In vitro* ubiquitination experiment was performed by incubating biotin-ubiquitin, E1, indicated E2, Mg^{2+} -ATP, IPP (inorganic pyrophosphatase), His-RNF186 and His-EPHB2 or His-EPHB3 recombinant proteins in $37^{\circ}C$ for 4 h, followed by western blot analysis of biotin-labeled ubiquitination. Data are representative of three independent experiments.

ubiquitin ligase for EPHB2 and EPHB3, we performed an *in vitro* ubiquitination experiment with recombinant

RNF186, EPHB2, or EPHB3 in a ubiquitination system also including Ub (biotin-ubiquitin), Mg^{2+} -ATP (adenosine

triphosphate), and IPP (inorganic pyrophosphatase), as well as E1 ligase and the E2 ligases UBE2H (ubiquitin conjugating enzyme E2 H), UBE2D2 (ubiquitin conjugating enzyme E2 D2), UBE2N (ubiquitin conjugating enzyme E2 N), or UBE2K (ubiquitin conjugating enzyme E2 K), as UBE2H was previously reported to serve as E2 ligase for RNF186 [35]. Indeed, RNF186 ubiquitinated EPHB2 and EPHB3 *in vitro* in the presence of UBE2H, which further confirmed that RNF186 is an E3 ligase for EPHB2 and EPHB3 (Figure 2J, K).

EFNB-induced autophagy is dependent on RNF186 and EPHB2

The findings that RNF186 could bind and ubiquitinate EPHB receptors and was required for the maintenance of basal level autophagy suggests that the EPHBs may be also involved in the activation of basal autophagy. To test this hypothesis, we first knockout *EPHB2* or *EPHB3* from the human colorectal cell line Ls174t, and examined the level of autophagy. Notably, *EPHB2*- but not *EPHB3*-deficient cells exhibited a considerable reduction in the expression of MAP1LC3B-II (Figure 3A, B), which was similar to the pattern observed in *RNF186* knockout cells (Figure 1B-D). Specifically, in the *EPHB2* knockout Ls174t cells, MAP1LC3B-II protein level was decreased by 51% and SQSTM1 increased by 1.65 fold compared with WT control cells (Figure 3A). We also confirmed that there was significantly reduced autophagosomes in *EPHB2* knockout Ls174t cells compared to WT control Ls174t cells at basal condition by electron microscopy (Fig. S1). The *EFNB1* gene encodes EFNB1 ligand protein for EPHB2, and *EFNB1* knockdown cells also had 49% of reduced MAP1LC3B-II level and the impaired capacity for intracellular bacterial clearance in Ls174t cells (Figure 3C, D). We therefore hypothesized that the deficient autophagy observed in *RNF186* knockout cells might rely on the EFNB-EPHB2 axis, while the EFNB-EPHB2 signaling pathway could potentially induce autophagy in an RNF186-dependent manner. To verify this hypothesis, we stimulated Ls174t cells with plate-coated ephrin-B1-Fc and ephrin-B2-Fc recombinant proteins and examined autophagy by probing MAP1LC3-II at multiple time points. Interestingly, both fusion proteins strongly increased the protein level of MAP1LC3B-II (Figure 3E).

To investigate whether the observed accumulation of MAP1LC3B-II was due to EFNB induced activation of autophagy or an inhibition of the lysosomal degradation pathway, we co-treated cells with plate-coated ephrin-B1-Fc and chloroquine (CQ). As expected, both treatments increase the amount of MAP1LC3B-II level, and notably, co-treatment with ephrin-B1-Fc and CQ induced significantly more MAP1LC3B-II accumulation than CQ treatment alone (Figure 3F). These results indicate that the observed accumulation of MAP1LC3B-II is due to EFNB-induced activation of autophagy rather than inhibition of the lysosomal degradation pathway. To further confirm that autophagy could be activated by EFNB1, we performed electron microscopy analysis of Ls174t cells treated with plate-coated Fc or ephrin-B1-Fc. Interestingly, ephrin-B1-Fc induced significantly more autophagosomes formation in the cells compared with Fc treatment (Figure 3G). To further understand the physiological function

of EFNB-induced autophagy, we co-stimulated cells with plate-coated ephrin-B1-Fc and salmonella, and found that co-stimulation induced higher levels of autophagy than single treatment (Figure 3H), and plate-coated ephrin-B1-Fc increase the clearance of intracellular salmonella compared with Fc treatment controls (Figure 3I). Overall, these data indicate that together with intracellular bacterial-induced autophagy, EFNB1-EPHB2-induced autophagy may help to facilitate the clearance of intracellular bacteria in colonic epithelial cells.

Based on our previous findings of reduced MAP1LC3-II accumulation and impaired bacterial clearance in *RNF186* knockout cells (Figure 1B-I), we next determined whether RNF186 or EPHB2 were required for EFNB-induced autophagy. The significantly reduced autophagy in *RNF186*- or *EPHB2*-knockout cells indicates that autophagy induced by EFNB1-EPHB2 signaling is fully dependent on RNF186 and EPHB2 (Figure 3J-K). Next, we employed endogenous immunofluorescence, which showed that ephrin-B1-Fc-induced autophagy was dependent on RNF186 and EPHB2 (Figure 3L-O). Consistently, ephrin-B1-Fc induced ATG16L1 aggregation in the WT cells, while there were significant less ATG16L1 puncta in the *EPHB2* knockout cells after ephrin-B1-Fc stimulation (Fig. S2A). These data provide further confirmation that EFNB1-induced autophagy is dependent on both EPHB2 and RNF186. Consistent with earlier data, ephrin-B1-Fc-induced MAP1LC3B puncta was significantly reduced in the *RNF186*^{A64T}-overexpressed cells compared to *RNF186* WT expressed cells, while *RNF186*^{R179X}-expressed cells showed significantly more MAP1LC3B puncta than WT *RNF186*-expressed cells after ephrin-B1-Fc stimulation (Fig. S2B). This data further indicates that *RNF186*^{A64T} is a loss-of-function mutant, and *RNF186*^{R179X} shows gain of function.

Ubiquitination of EPHB2 at residue K892 by RNF186 is required for EFNB1-EPHB2-induced autophagy

As RNF186 is an E3 ligase for EPHB2 (Figure 2), and both RNF186 and EPHB2 are required for EFNB1-induced autophagy, we hypothesized that RNF186-mediated EPHB2 ubiquitination may play a critical role in this process. Consistent with our hypothesis, ephrin-B1-Fc can induce EPHB2 ubiquitination, which is dependent on RNF186 (Figure 4A). To further understand whether RNF186-mediated EPHB2 ubiquitination plays an important role in EFNB1-EPHB2-induced autophagy, we performed mass spectrometry analysis to further explore possible EPHB2 ubiquitination sites catalyzed by RNF186. In this analysis, two EPHB2 lysine sites were identified as being ubiquitinated by RNF186, K788 and K892. Both of these sites were highly conserved across species (Figure 4B, C). Moreover, we found that in the lysine-to-arginine mutant *EPHB2*^{K892R}, but not *EPHB2*^{K788R}, the ubiquitination of EPHB2 by RNF186 was abolished (Figure 4D). Restoration of the WT *EPHB2* or *EPHB2*^{K788R}, but not *EPHB2*^{K892R} rescued the ephrin-B1-Fc-induced autophagy in *EPHB2* knockout cells (Figure 4E). This data indicates that ubiquitination of EPHB2 at K892 by RNF186 is essential for EFNB1-induced autophagy. Consistent with these findings, intracellular bacteria grew significantly faster in *EPHB2*^{K892R}

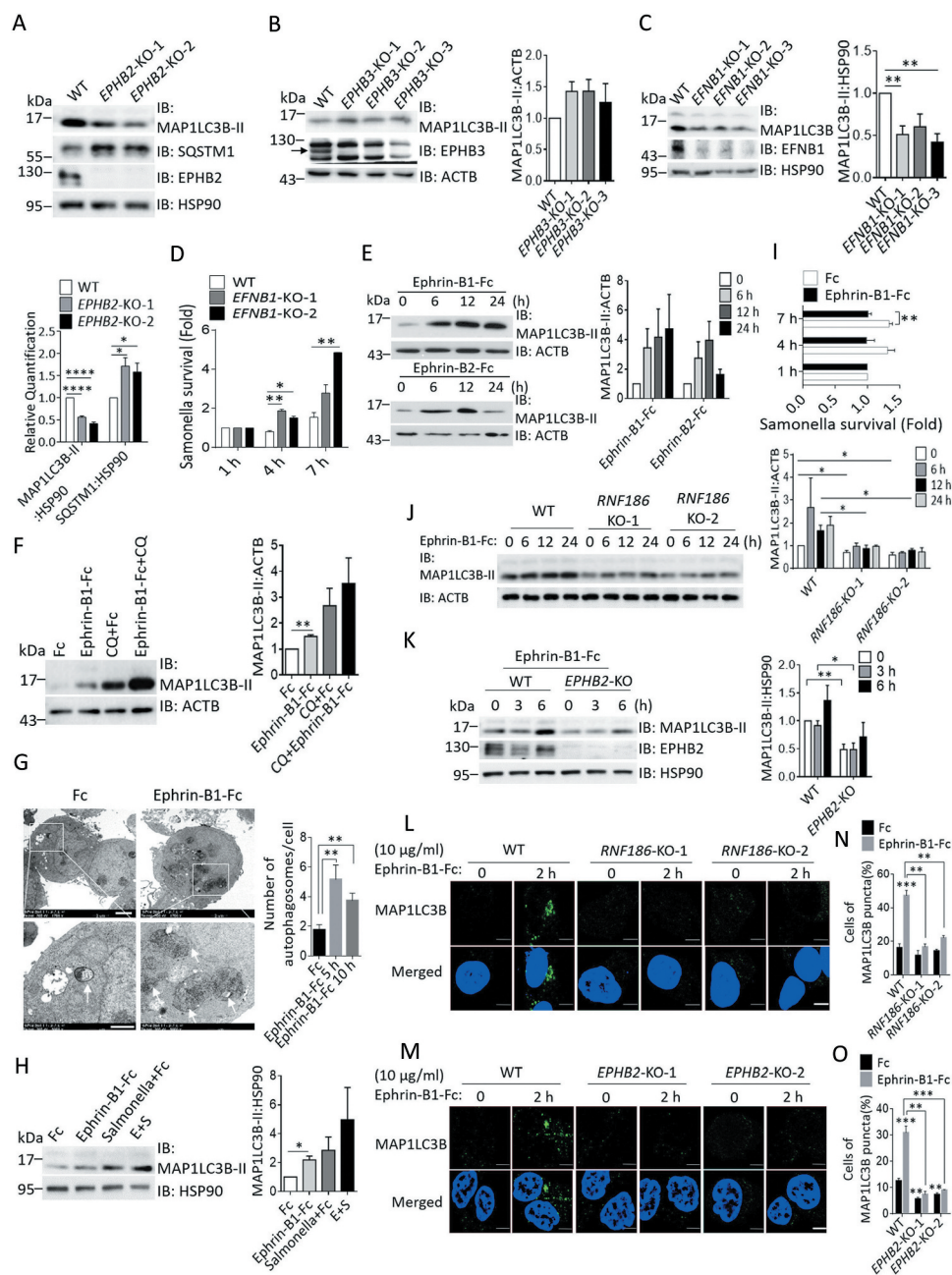


Figure 3. EFN-induced autophagy in colonic epithelial cells is dependent on RNF186 and EPHB2. (A) Lysates of WT or *EPHB2*-KO cells were analyzed by western blot for the indicated proteins. Densitometry quantification from three independent experiments was shown in the bottom panel. (B and C) Lysates of WT or *EPHB3*-KO (B) or *EFNB1*-KO (C) Ls174t cells were analyzed by western blot for the indicated proteins. Densitometry quantification from three independent experiments was shown in the right panel. (D) Intracellular Salmonella number of control cells and two *EFNB1*-KO cells was counted by serial dilution and plating after bacterial infection. (E) Ls174t cells were treated with 10 μ g/ml plate-coated Fc (0 time point) or ephrin-B1-Fc or ephrin-B2-Fc as indicated, followed by western blot analysis of the indicated proteins. Densitometry quantification from three independent experiments was shown in the right panel. (F) Ls174t cells were stimulated with 10 μ g/ml plate-coated Fc, ephrin-B1-Fc, 50 μ M chloroquine or ephrin-B1-Fc plus chloroquine for 6 h, followed by western blot analysis of the indicated proteins. Densitometry quantification from three independent experiments was shown in the right panel. (G) Ls174t cells were treated with 10 μ g/ml plate-coated Fc (0 time point) or ephrin-B1-Fc for the indicated time, followed by electron microscopy analysis. White arrow indicates autophagosome in the cells. Quantitatively analysis of autophagosomes in each cell was shown on the right panel. Top panel scale bar: 2 μ m; bottom panel scale bar: 1 μ m. (H) Ls174t cells were treated with 10 μ g/ml plate-coated Fc or ephrin-B1-Fc, followed by Salmonella stimulation for 4 h and western blot analysis. "E + S" represent "Ephrin-B1-Fc + Salmonella". Densitometry quantification from three independent experiments was shown in the right panel. (I) Intracellular salmonella number analysis was shown as described in METHODS. (J-K) WT, *RNF186*-KO cells (J) or *EPHB2*-KO cells (K) were treated with 10 μ g/ml plate-coated Fc (0 time point) or ephrin-B1-Fc as indicated, followed by western blot analysis of the indicated proteins. Densitometry quantification from three independent experiments was shown in the right panel. (L and M) WT or *RNF186*-KO Caco2 cells (L) and WT or *EPHB2*-KO Ls174t cells (M) were stimulated with 10 μ g/ml plate-coated Fc or ephrin-B1-Fc for 2 h, and localization of endogenous MAP1LC3B-II labeled by green fluorescence was examined by confocal microscopy. Scale bar: 5 μ m. (N and O) Quantification of cells with puncta of MAP1LC3B-II was shown in the right for (L) and (M). WT: wild type; KO: knockout; CQ: chloroquine. All error bars represent SEM of technical replicates. *: $P < 0.05$, **: $P < 0.01$, ***: $P < 0.001$, ****: $P < 0.0001$ based on two-sided unpaired T test (A-K, N and O). Densitometry quantification of A-F, H-K were based on three independent experiments. Data are representative of three independent experiments.

restored cells than that in WT EPHB2-restored cells (Figure 4F). Furthermore, we found that WT EPHB2 interacted with MAP1LC3B in 293 T cells (Figure 4G) while EPHB2^{K892R} showed reduced interaction with MAP1LC3B (Figure 4H). These data indicate that upon EFN1 stimulation, ubiquitination of EPHB2 at K892 by RNF186 is a critical step in the activation of autophagy.

EFNB1-EPHB2-induced autophagy is MTOR-independent

It was well known that MTOR (mechanistic target of rapamycin kinase) inhibits canonical autophagy, and inhibition of MTOR pathway activates canonical autophagy [10,36,37]. Therefore, we explored whether EFN1-EPHB2-induced autophagy was dependent on MTOR inhibition. Surprisingly, plate-coated ephrin-B1-Fc treatment induced phosphorylation of MTOR and RPS6 (ribosomal protein S6), suggesting inhibition of canonical autophagy. However, at later time point following stimulation we observed the upregulation of MAP1LC3B-II protein levels (Figure 5A), indicating that EFN1-induced autophagy is independent of MTOR activity. Furthermore, ULK1 inhibitor SBI-0206965 and PtdIns3K (Class III phosphatidylinositol 3-kinase) inhibitors 3-methyladenine (3-MA) and wortmannin blocked ephrin-B1-Fc-induced autophagy, which indicates that activation of ULK1 and PtdIns3K are required for this EFN1-induced autophagy pathway (Figure 5B-D). Consistent with this, ephrin-B1-Fc induced MAP1LC3B aggregation was greatly decreased following treatment with 3-MA or wortmannin, as assessed by immunofluorescence (Figure 5E). VPS34-IN1, a potent and highly selective PtdIns3K inhibitor which does not significantly inhibit the isoforms of class I as well as class II PI3Ks, also inhibited ephrin-B1-Fc induced autophagy, which indicates that PtdIns3K is exactly involved in this process (Figure 5F). As expected, depletion of ATG5 (autophagy related 5) significantly diminished the ephrin-B1-Fc-induced autophagy (Figure 5G), which indicates that this pathway is dependent on ATG5. In sum, these results indicate that EFN1-EPHB2-induced autophagy is independent of MTOR activity, but is dependent upon ULK1, PtdIns3K and ATG5.

Rnf186- and ephb2-deficient mice are susceptible to DSS-induced colitis

We have demonstrated that RNF186 is involved in the regulation of EFN1-EPHB2-induced autophagy, and it has previously been well-demonstrated that dysregulation of autophagy plays an important role in the pathogenesis of IBD. Furthermore, RNF186 has been reported to associate with UC susceptibility. Therefore, we examined whether *rnf186*^{-/-} mice exhibited a spontaneous colitis phenotype. We did not observe any gross or histological abnormalities in the large intestine of *rnf186*^{-/-} mice to suggest spontaneous colitis (Fig. S3A and S3B). Moreover, comparable levels of pro-inflammatory gene expression (Fig. S3C) and intestinal permeability were observed between *Rnf186*^{+/-} and *rnf186*^{-/-} mice (Fig. S3D). Although *ephb2*^{-/-} and *ephb3*^{-/-} mice harbored mispositioned Paneth cells that were scattered along the crypt-villus axis rather than concentrated in crypts [22,23], there

were no obvious changes in Paneth cell localization in *rnf186*^{-/-} mice compared with the control mice (Fig. S3E).

We next explored the role of RNF186 in a dextran sodium sulfate (DSS)-induced colitis model. Notably, *rnf186*^{-/-} mice exhibited significantly more rapid weight loss compared to *Rnf186*^{+/-} control mice (Figure 6A). Additionally, on gross analysis DSS-treated *rnf186*^{-/-} mice exhibited a greater level of colonic shortening, and increased thickening of the muscular layer, compared to control mice (Figure 6B). Histopathological analysis of colon sections revealed more severe epithelial damage, including crypt dropout, leukocytic infiltration extending into the muscularis mucosae, and edematous thickening of the mucosae in DSS-treated *rnf186*^{-/-} mice, as compared to *Rnf186*^{+/-} controls (Figure 6C). The expression of pro-inflammatory genes, including genes with well-described roles in colitis pathogenesis, were significantly increased in colon samples from *rnf186*^{-/-} mice compared to controls (Figure 6D). Colonic epithelial cells from *rnf186*^{-/-} mice also showed decreased MAP1LC3B-II protein level compared to that from control mice following DSS treatment (Figure 6E). These data indicate that deficiency of *Rnf186* results in a more severe colitis phenotype, which is due to reduced autophagy in colonic epithelial cells.

From our molecular mechanistic study, we found that RNF186 was required for EFN1-EPHB2-induced autophagy in colonic epithelial cells. In order to further confirm the role of this pathway in intestinal homeostasis, we generated *ephb2*^{-/-} mice (Fig. S3F), and examined the susceptibility of *ephb2*^{-/-} mice to DSS-induced colitis. Consistent with the findings in *rnf186*^{-/-} mice, *ephb2*^{-/-} mice exhibited significantly more rapid weight loss compared to *Ephb2*^{+/+} control littermates (Figure 6F), and all of *ephb2*^{-/-} mice died before day 9 after DSS treatment, while *Ephb2*^{+/+} control mice shown approximately 44% death rate in the colitis model (Figure 6G). The colon length of *ephb2*^{-/-} mice was significantly shorter compared to *Ephb2*^{+/+} control mice, and histological analysis of the colon sections revealed significantly more severe epithelial damage and inflammation in DSS-treated *ephb2*^{-/-} mice, compared to WT mice (Figure 6H, Figure 6I). Pro-inflammatory gene expression in colon samples from *ephb2*^{-/-} mice was significantly higher than in samples from *Ephb2*^{+/+} mice (Figure 6J). Immunoblot of MAP1LC3B analysis further revealed a lower level of MAP1LC3B-II in the colonic epithelial cells of DSS-treated *ephb2*^{-/-} mice than that in similarly treated control mice (Figure 6K). Overall, these data further confirmed the important role of EFN1-EPHB2-induced autophagy in intestinal homeostasis.

Ephrin-B1-Fc has therapeutic activity in DSS-induced colitis

The susceptibility of *rnf186*^{-/-} and *ephb2*^{-/-} mice to DSS-induced colitis was attributed to the defective activation of autophagy in colonic epithelial cells in response to EFN1-EPHB2 signaling. Therefore, we speculated that EFN1-induced autophagy might represent a promising therapeutic modality for colitis patients. To test this hypothesis, we intraperitoneally injected Fc or Mmephrin-B1-Fc recombinant protein into WT mice with DSS-induced colitis, and

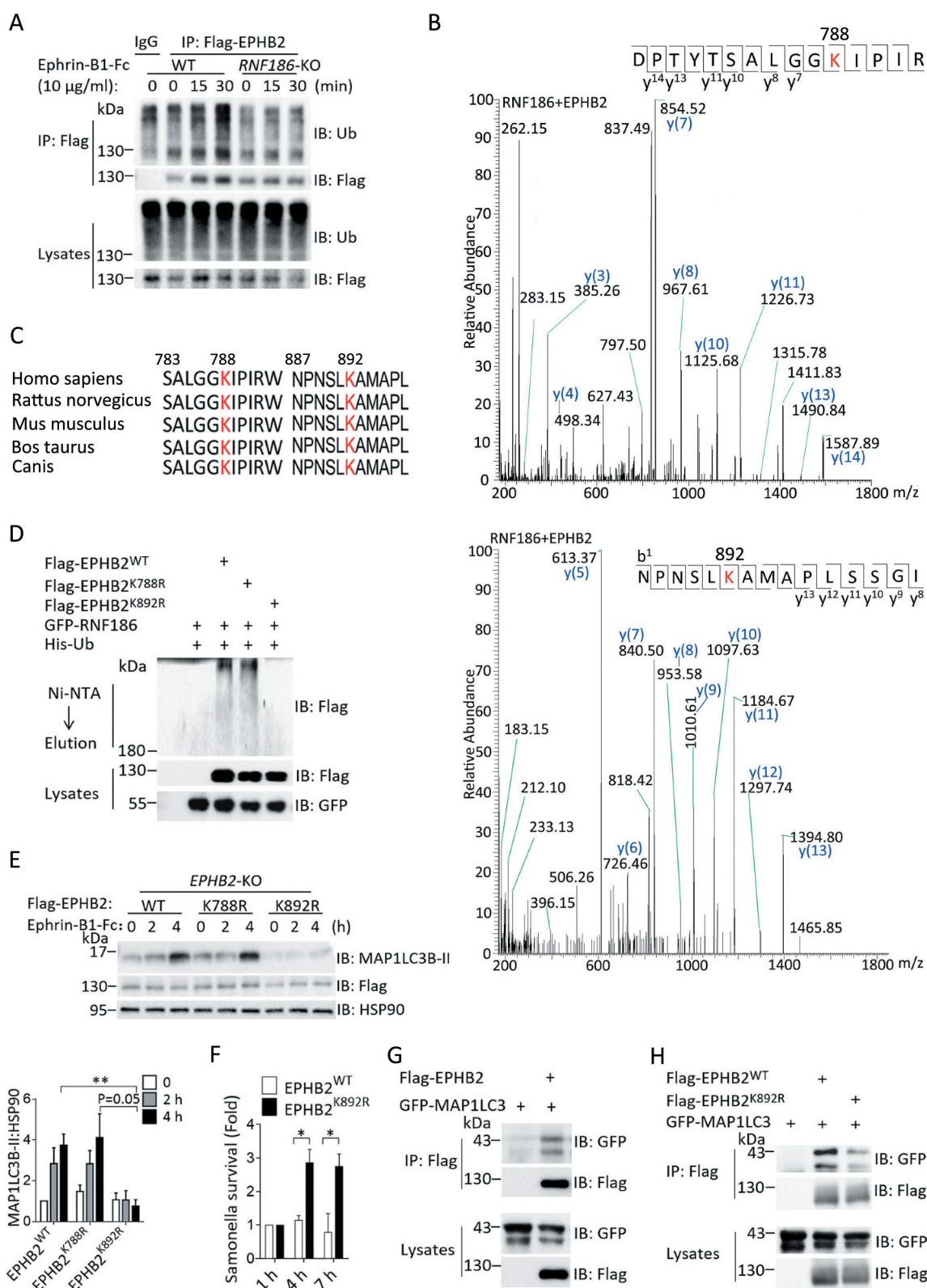


Figure 4. Ubiquitination at Lys92 in EPHB2 by RNF186 is essential for EFN1-induced autophagy. (A) Flag-tagged WT EPHB2 was stable-expressed into WT or *RNF186*-KO Ls174t cells, followed by the stimulation with 10 µg/ml plate-coated Fc (0 time point) or ephrin-B1-Fc for the indicated time. Cell lysates were immunoprecipitated by anti-Flag antibody, followed by western blot analysis of the indicated proteins. (B) Mass spectrometry identification of EPHB2 ubiquitination sites by RNF186 was shown. (C) The conservative analysis of EPHB2 788th and 892th sites among different species. (D) 293 T cells were transfected with the indicated plasmids, followed by ubiquitination experiment described as in the METHODS. (E) Flag-tagged EPHB2, EPHB2^{K788R} or EPHB2^{K892R} were restored into *EPHB2*-KO Ls174t cells, followed by the stimulation with 10 µg/ml plate-coated Fc (0 time point) or ephrin-B1-Fc for the indicated time, and cell lysates were analyzed by western blot. Densitometry quantification from three independent experiments was shown in the bottom panel. (F) Intracellular *Salmonella* number of EPHB2 or EPHB2^{K892R} restored Ls174t cells was counted by serial dilution and plating after bacterial infection. (G and H) 293 T cells were transfected as indicated, and cell lysates were immunoprecipitated by anti-Flag antibody, followed by western blot analysis of the indicated proteins. WT: wild type; KO: knockout. All error bars represent SEM of technical replicates. *: $P < 0.05$, **: $P < 0.01$, ***: $P < 0.001$, ****: $P < 0.0001$ based on two-sided unpaired T test (E and F). Data are representative of three independent experiments.

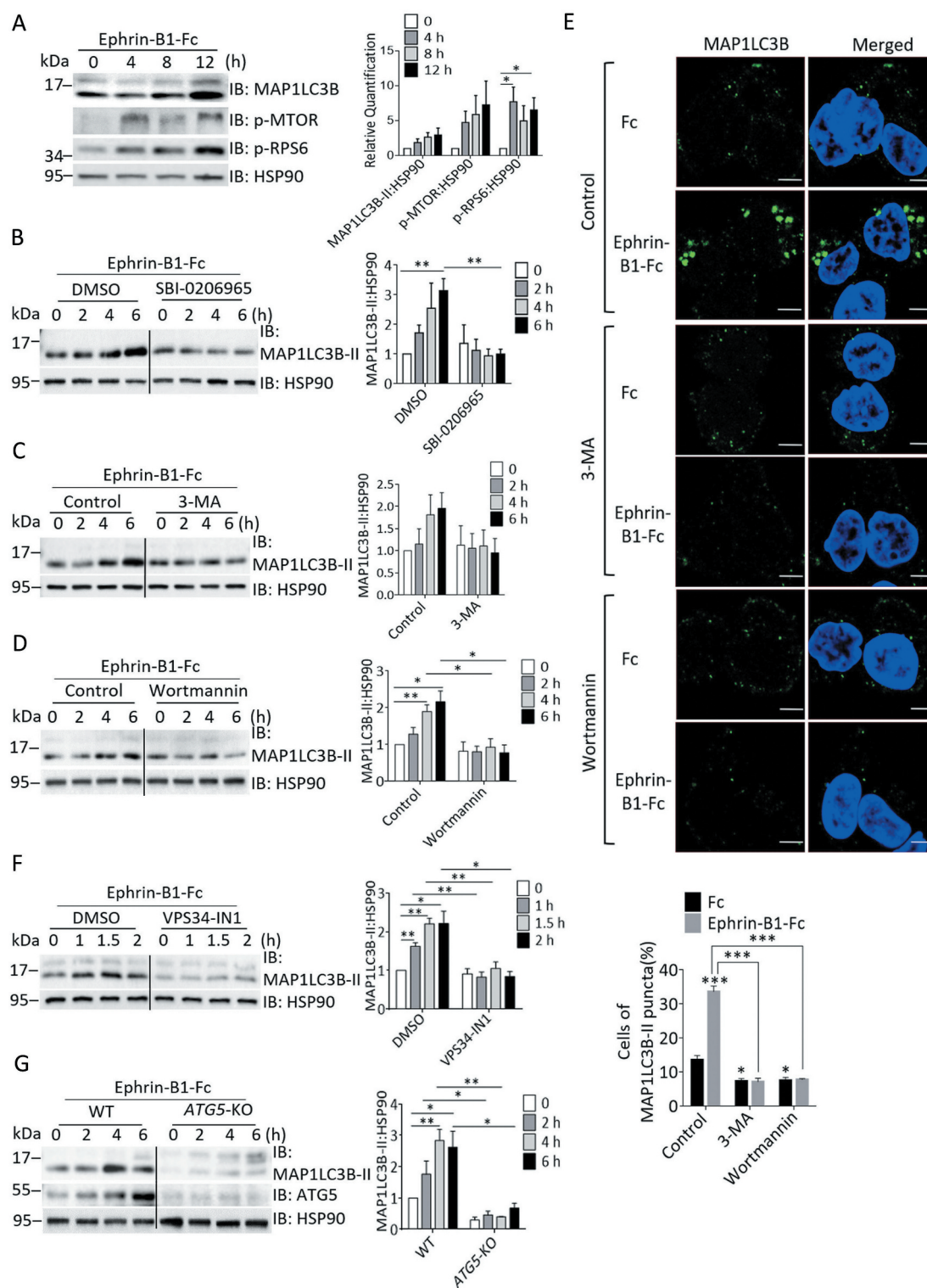


Figure 5. EFNB1-induced autophagy is independent of MTOR inhibition. (A) Ls174t cells were treated as indicated, followed by western blot analysis of the indicated proteins. Densitometry quantification from three independent experiments was shown in the right panel. (B-D) Ls174t cells were pretreated with SBI-0206965 (10 μ M) (B), 3-MA (5 mM) (C) or wortmannin (100 nM) (D) for 1 h, followed by the treatment of plate-coated Fc or ephrin-B1-Fc (10 μ g/ml) in presence of the inhibitors for the indicated time. Cell lysates were analyzed by western blot for the indicated proteins. Densitometry quantification from three independent experiments was shown in the right panel. (E) Ls174t cells were pretreated with DMSO, 3-MA (5 mM) or wortmannin (100 nM) for 1 h, followed by plate-coated Fc or ephrin-B1-Fc (10 μ g/ml) for 2 h in presence of the inhibitors and followed by confocal microscopy analysis of MAP1LC3B puncta. Quantification of cells with puncta of MAP1LC3B-II was shown in the bottom panel. Scale bar: 5 μ m. (F) Ls174t cells were pretreated with VPS34-IN1 (2 μ M) for 1 h, followed by the treatment of plate-coated Fc or ephrin-B1-Fc (10 μ g/ml) in presence of the inhibitor for the indicated time. Cell lysates were analyzed by western blot for the indicated proteins. Densitometry quantification was shown in the right panel. (G) Control-gRNA or ATG5-gRNA infected Ls174t cells were treated with 10 μ g/ml plate-coated Fc (0 time point) or ephrin-B1-Fc, followed by western blot analysis of the indicated proteins. Densitometry quantification from three independent experiments was shown in the right panel. WT: wild type; KO: knockout; 3-MA: 3-methyladenine. All error bars represent SEM of technical replicates. *: $P < 0.05$, **: $P < 0.01$, ***: $P < 0.001$, ****: $P < 0.0001$ based on two-sided unpaired T test (A-G). Densitometry quantification of A-D and F-G were based on three independent experiments. Data are representative of three independent experiments.

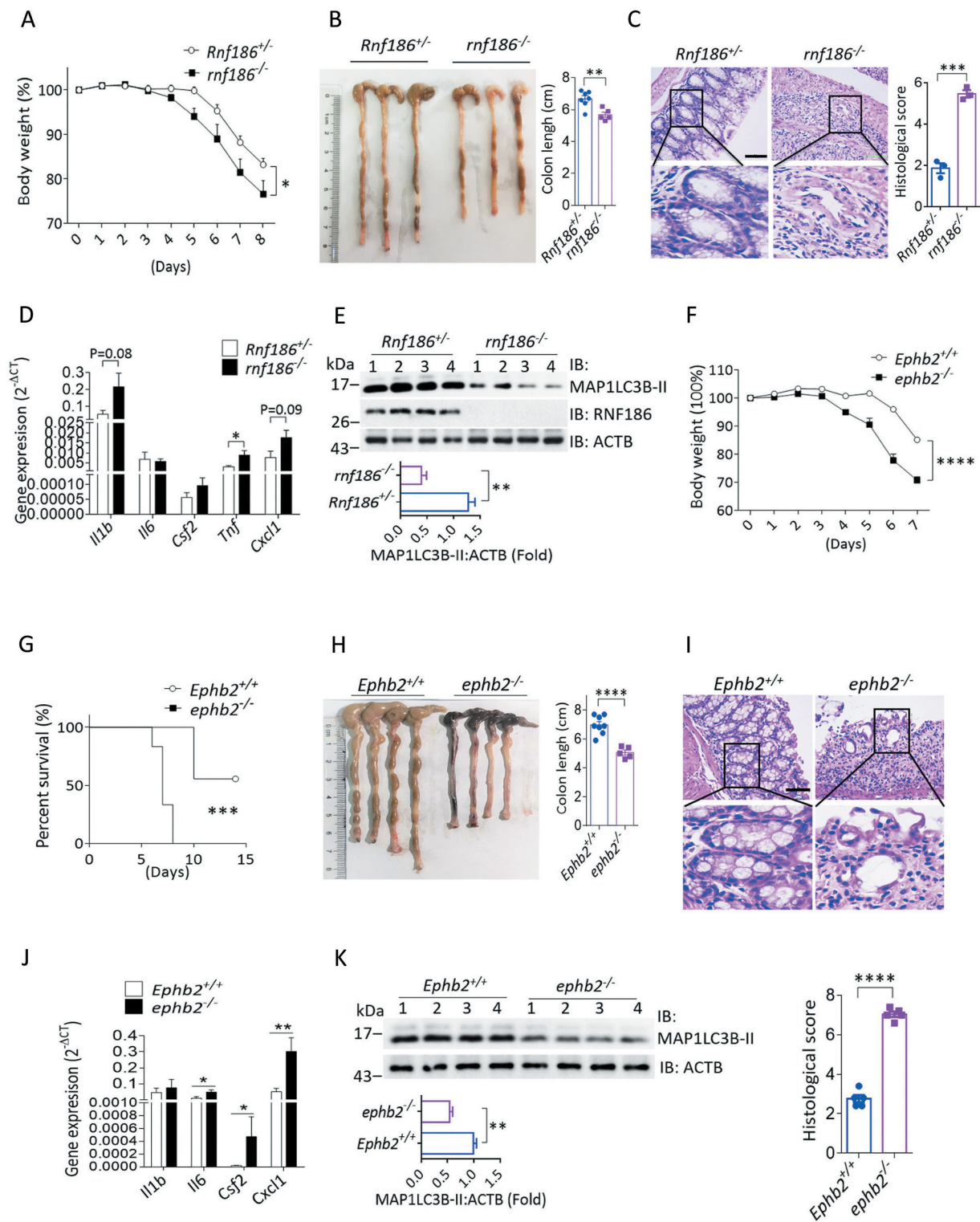


Figure 6. *Rnf186*^{-/-} and *ephb2*^{-/-} mice were susceptible to DSS-induced colitis. (A) *Rnf186*^{+/-} or *rnf186*^{-/-} mice were treated with 2% DSS in the drinking water for 7 days, and changed to normal water as described in the Methods. Weight curve was shown. *Rnf186*^{+/-} n = 7, *rnf186*^{-/-} n = 5. (B) Representative colon picture of DSS-treated *Rnf186*^{+/-} and *rnf186*^{-/-} mice was shown (left). Colon length of *Rnf186*^{+/-} and *rnf186*^{-/-} mice after DSS treatment was quantified (right). *Rnf186*^{+/-} n = 7, *rnf186*^{-/-} n = 5. (C) Hematoxylin-eosin staining of transversal sections of colon sample from DSS-treated *Rnf186*^{+/-} and *rnf186*^{-/-} mice was shown. Histological score was shown in the right panel, which is according to the method described in the METHODS. Scale bar: 50 μ m. n = 3. (D) mRNA was isolated from colonic samples of DSS-treated *Rnf186*^{+/-} and *rnf186*^{-/-} mice, and gene expression was analyzed by RT and real-time PCR. n = 6. (E) Colonic epithelial cells from *Rnf186*^{+/-} and *rnf186*^{-/-} mice were isolated at day 8, followed by western blot analysis of indicated proteins. Densitometry quantitative analysis of MAP1LC3B-II/ACTB was shown in the bottom panel. (F and G) *Ephb2*^{+/-} or *ephb2*^{-/-} mice were treated with 2% DSS in drinking water for 6 days, and changed to normal water. Weight curve and survival rate were shown. *Ephb2*^{+/-} n = 9, *ephb2*^{-/-} n = 6. (H) The representative image of colon was shown (left), and the colon length was shown on the right panel. *Ephb2*^{+/-} n = 8, *ephb2*^{-/-} n = 5. (I) Hematoxylin-eosin staining of transversal sections of colon sample from DSS-treated *Ephb2*^{+/-} or *ephb2*^{-/-} mice were shown. Histological score was shown in the bottom panel, which is according to the method described in the METHODS. Scale bar: 50 μ m. n = 5. (J) mRNA was isolated from colonic samples of DSS-treated *Ephb2*^{+/-} or *ephb2*^{-/-} mice, and gene expression was analyzed by qRT-PCR. *Ephb2*^{+/-} n = 9, *ephb2*^{-/-} n = 5. (K) Colonic epithelial cells from *Ephb2*^{+/-} or *ephb2*^{-/-} mice were isolated at day 7, followed by western blot analysis of indicated proteins. Densitometry quantitative analysis of MAP1LC3B-II/ACTB was shown in the bottom panel. Colonic samples were harvested at day 8 for A-E, and day 7 for F, H-K. *: P < 0.05, **: P < 0.01, ***: P < 0.001, ****: P < 0.0001 based on two-way ANOVA (A and F), two-sided unpaired T test (B-E, H-K) and Log-rank E(Mantel-Cox) test for (G). All error bars represent SEM of technical replicates. Data are representative of three independent experiments.

examined the impact on colitis disease severity. Notably, Mmephrin-B1-Fc-treated mice exhibited a slower rate of weight loss and more rapid recovery compared with Fc-treated control mice (Figure 7A). Histopathological analysis of colon samples revealed that Mmephrin-B1-Fc treatment attenuated colonic epithelial damage compared with control Fc treatment (Figure 7B). The colon length of Mmephrin-B1-Fc-treated mice was also longer than controls (Figure 7C). Consistent with our *in vitro* findings, we observed a higher level of MAP1LC3B-II level in the colonic epithelial cells from Mmephrin-B1-Fc-treated mice, compared with Fc-treated mice (Figure 7D). To further clarify whether the ameliorative treatment of Mmephrin-B1-Fc on DSS-induced colitis is indeed achieved through EPHB2, we employed *ephb2*^{-/-} mice to reassess the effect of Mmephrin-B1-Fc on DSS-induced colitis. Interestingly, administration of Mmephrin-B1-Fc significantly attenuated DSS-induced colitis phenotype in *Ephb2*^{+/+} mice but had little effect on *ephb2*^{-/-} mice, as assessed by weight loss and colon length (Figure 7E-F). Histopathological and proinflammatory gene expression analysis of colon sections also demonstrated a therapeutic effect of Mmephrin-B1-Fc on *Ephb2*^{+/+} mice but not on *ephb2*^{-/-} mice (Figure 7G-H). Immunoblot analysis further indicated that administration of Mmephrin-B1-Fc promoted autophagy in the colonic epithelial cells of *Ephb2*^{+/+} mice but not *ephb2*^{-/-} mice (Figure 7I). Taken together, these data indicate that ephrin-B1-Fc exerts a therapeutic effect on DSS-induced colitis by increasing RNF186- and EPHB2-associated autophagy in colonic epithelial cells, and thereby implies that this strategy may also have potential for the treatment of human ulcerative colitis.

Discussion

In this study, we have provided evidence that the E3 ligase RNF186 is indispensable for EFNB-induced basal autophagy and the clearance of intracellular pathogens in colonic epithelial cells. This newly identified mechanism is essential for the maintenance of intestinal hemostasis and reflects an important mechanism of host defense against intracellular pathogens in the intestinal mucosal immune system. Moreover, we found that the dysregulation of this pathway leads to defective autophagy and increases susceptibility to UC (Fig. S4). Moreover, we have provided evidence that treatment with the recombinant protein ephrin-B1-Fc ameliorates DSS-induced colitis and exerts its therapeutic effect by inducing autophagy in colonic epithelial cells, thereby suggesting that this recombinant protein could potentially be used to treat human IBD.

The potential role of autophagy in IBD susceptibility has been well established, and many genetic risk polymorphisms have been mapped to various autophagy-related genes, including *Atg16l1* [11], *ULK1* [13], *IRGM* and *GPR65* (G protein-coupled receptor 65) [14,38,39], among others. Additionally, the relationship between defects in autophagy-mediated intracellular bacterial clearance, innate immune activation, and IBD pathogenesis have become increasingly well understood. In this study, we identified a novel autophagy activation pathway induced by EFNB1 in colonic

epithelial cells, which is required for efficient intracellular pathogen clearance. Interestingly, ephrin-B1-Fc mediated autophagy in colonic epithelial cells is independent of MTOR. It is well known that MTOR inhibits canonical autophagy, and inhibition of MTOR leads to activation of the canonical autophagy pathway [36,37,40,41]. Importantly, however, non-canonical MTOR-independent autophagy pathways have also been previously identified [42–45]. Here, we found that EFNB1-induced autophagy activation is independent of MTOR status, but is dependent on EPHB2, RNF186, ULK1, PtdIns3K and ATG5 molecules. However, the exact molecular mechanism of signal transduction for EFNB1-induced autophagy remains unclear, and merits further investigation. A recent study by others reported that RNF186 maintains gut homeostasis by controlling ER stress in colonic epithelia [32], which differs from our finding that RNF186 is mainly involved in the regulation of autophagy in intestinal epithelial cells. It is worth noting, however, that ER stress and autophagy are intimately linked, and it is widely accepted that ER stress can activate autophagy via multiple pathways, and autophagy can also regulate ER stress under certain circumstances [46–49]. Therefore, it is possible that in certain stimulus-dependent contexts RNF186 may also be involved in ER stress responses, which merits further investigation in the future.

Although the mechanisms of IBD pathogenesis have been extensively investigated, and many genetic and environmental factors underlying IBD have been described, there remains significant unmet clinical need for improved therapeutic strategies for IBD. Given that autophagy has been reported to play a key role in the pathogenesis of IBD, prior case reports and at least one clinical trial have reported experimental use of rapamycin for the treatment of IBD. One recent case report has described a single patient having achieved sustained remission from Crohn's disease, while a double-blind placebo-controlled clinical trial with everolimus (another MTOR inhibitor) for the treatment of CD was terminated early after a negative interim analysis [50–52]. It is widely acknowledged that MTOR is not only involved in controlling activation of autophagy, but also affects cell proliferation, cell growth, and other important biological pathways. For this reason, pharmacological induction of autophagy by MTOR inhibition may induce numerous off-target effects. Thus, there is an ongoing effort to identify MTOR-independent autophagy activators for the treatment of IBD and other autophagy-related disorders, such as the experimental use of carbamazepine-autophagy inducer independent of MTOR inhibition for the treatment of α 1-antitrypsin (α 1AT) deficiency [53]. In this study, we provide evidence that EFNB1-induced autophagy in intestinal epithelial cells is MTOR-independent and the ephrin-B1-Fc recombinant protein has a therapeutic effect on DSS-induced colitis, which it exerts via induction of autophagy in colonic epithelial cells. These data suggest that the recombinant protein ephrin-B1-Fc may have promise as a novel therapeutic strategy for the treatment of IBD, and the MTOR-independent mechanism of action suggests that this strategy may be associated with fewer undesirable off-target effects than MTOR-targeted agents.

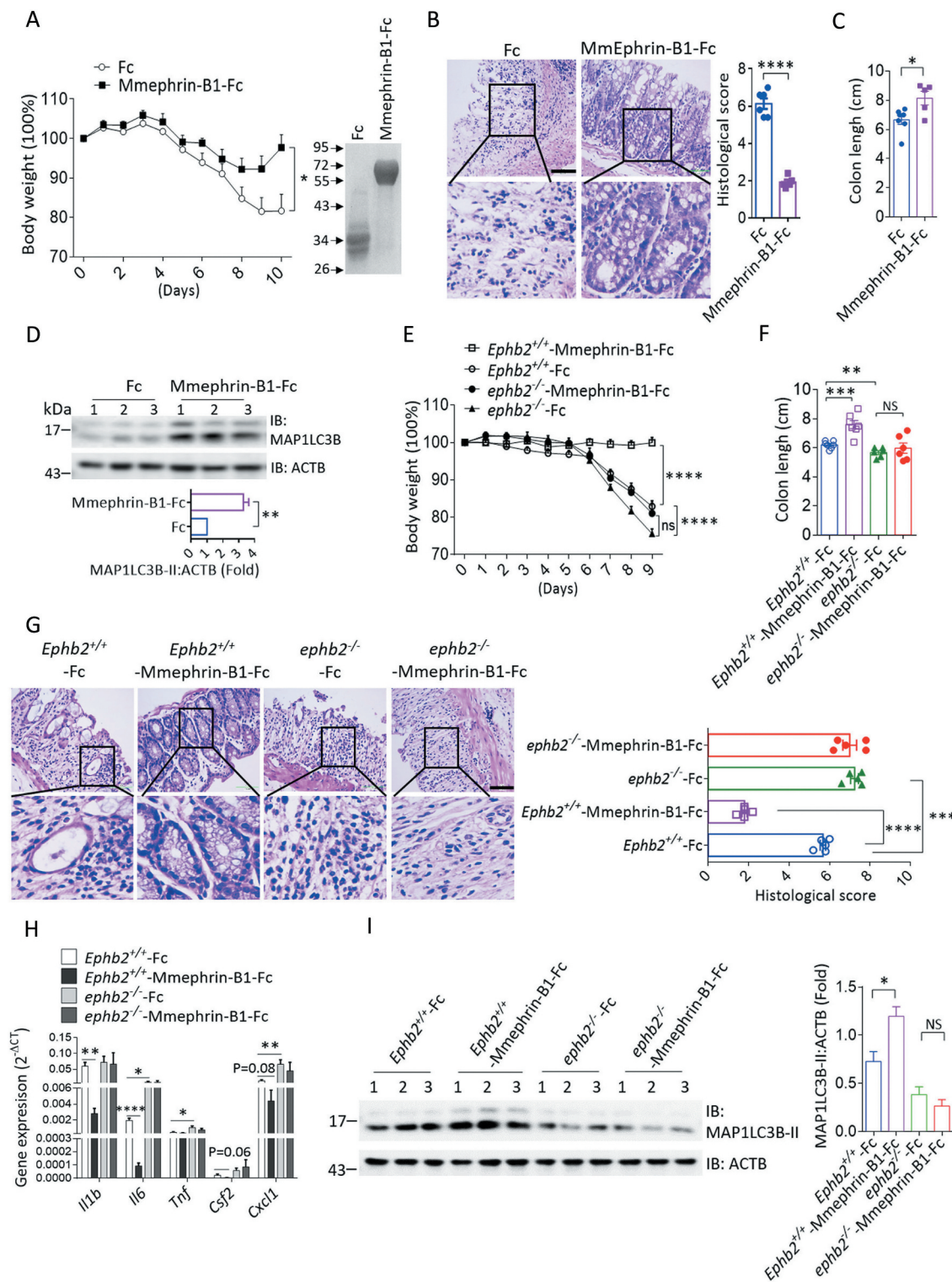


Figure 7. Ephrin-B1-Fc recombinant protein has therapeutic effect for DSS-induced colitis. (A) WT C57BL/6 mice intraperitoneally injected with 50 μ g Fc or Mmephrin-B1-Fc were treated with 2% DSS in the drinking water for 7 days as described in the METHODS, and weight curve was shown. Fc n = 7, Mmephrin-B1-Fc n = 5. Purified Fc and Mmephrin-B1-Fc recombinant proteins were shown on the right panel. (B) Hematoxylin-eosin staining of transversal sections of colon sample from Fc or Mmephrin-B1-Fc injected mice was shown (DSS treatment for 7 days). Histological score was shown in the right panel. Scale bar: 50 μ m. n = 6/5. (C) Colon length of Fc or Mmephrin-B1-Fc injected mice after DSS treatment was quantified. n = 7/5. (D) Colonic epithelial cells from Fc-treated mice or Mmephrin-B1-Fc-treated mice were isolated at day 7, followed by western blot analysis of indicated proteins. Densitometry quantitative analysis of MAP1LC3B-II/ACTB was shown in the bottom panel. (E) *Ephb2*^{+/+} mice or *ephb2*^{-/-} mice intraperitoneally injected with 100 μ g Fc or Mmephrin-B1-Fc were treated with 2% DSS in the drinking water for 7 days as described in the METHODS, and weight curve was shown. *Ephb2*^{+/+}-Fc n = 7, *Ephb2*^{+/+}-Mmephrin-B1-Fc n = 7, *ephb2*^{-/-}-Fc n = 6, *ephb2*^{-/-}-Mmephrin-B1-Fc n = 5. (F) *Ephb2*^{+/+} or *ephb2*^{-/-} mice were treated as in E, and quantification of colon length was shown. n = 7/7/6/5. (G) Hematoxylin-eosin staining of transversal sections of colon sample from Fc or Mmephrin-B1-Fc injected *Ephb2*^{+/+} or *ephb2*^{-/-} mice was shown. Histological score was shown in the right panel, which is according to the method described in the METHODS. Scale bar: 50 μ m. n = 5. (H) mRNA was isolated from colon samples of DSS-treated mice, and gene expression was analyzed by qRT-PCR. n = 7/6/7/6. (I) Colonic epithelial cells from Fc-treated mice or Mmephrin-B1-Fc-treated mice were isolated at day 7, followed western blot analysis of indicated proteins. Densitometry quantitative analysis of MAP1LC3B-II/ACTB was shown in the right panel. Colonic samples were harvested at day 10 for A-C, and day 9 for E-I. *; P < 0.05. **; P < 0.01. ***; P < 0.001. ****; P < 0.0001 based on two-way ANOVA (A and E) and two-sided unpaired T test (B, C, D, F, G, H and I). All error bars represent SEM of technical replicates. Data of A-D are representative of three independent experiments, and data of E-I are representative of two independent experiments.

As noted previously, EFN-EPHB signaling has been reported to regulate cell migration, progenitor cell proliferation, cancer initiation and metastasis in the intestinal epithelium [19,23–25]. Several reports have suggested that EPHB2 is involved in autophagy and cancer cell apoptosis, however the precise mechanism by which EPHB2 regulates autophagy has remained unknown [34,54,55]. The EFN1-EPHB2-induced autophagy pathway that we have identified here will not only help to further understand the molecular and cellular mechanisms of IBD pathogenesis, but may also provide a novel therapeutic strategy for the treatment of IBD. It would be very useful to further explore the role of EFN1-EPHB2-induced autophagy in intestinal epithelial cells, including the underlying signal transduction mechanism, as well as the elucidation of other molecules involved in this pathway, and the biological differences between EFN1-EPHB2 signaling and other stimuli that induce autophagy (e.g., intracellular pathogens).

Materials and methods

Control or UC patients' biopsy samples

Control and UC patients' biopsy samples were gotten from department of Gastroenterology, People's Hospital of Wuhan University. This study followed the guidelines set forth by the Declaration of Helsinki and passed the review of the Ethics Committee of People's Hospital of Wuhan University and Huazhong University of Science and Technology. All study participants have signed a written informed consent form.

Mice

The *rnf186*^{-/-} mouse and *ephb2*^{-/-} mouse were made by Cyagen Biosciences Inc. by CRISPR-Cas9 technique as demonstrated in Fig. S3A and S3F. The gRNAs sequence to deplete *Rnf186* are as follows: gRNA1: TCATTGCCTTGGGGCCACCGGG; gRNA2: CCCCTGTCCGCTGTGCCGAAAGG. The 188-bp DNA fragment was depleted by these two gRNA, which was confirmed by genotyping. The depletion of the 188-bp DNA fragment resulted in a frameshift for the rest of the *Rnf186* cDNA. The gRNAs sequence to deplete *Ephb2* are as follows: gRNA1: GCTCAGAAGTCCACGTGG; gRNA2: GCTGGGTGCCCTATTAGTGTGG. The 4591-bp DNA fragment was depleted by these two gRNA, which was confirmed by genotyping. The depletion of the 4591-bp DNA fragment resulted in a frameshift for the rest of the *Ephb2* cDNA. To avoid possible off-target editing of the genome, the mice were breed six generation with mice of C57BL/6 background before perform any experiments. Experimental protocols were approved by the Institutional Animal Care and Use Committee of the Tongji Medical College, Huazhong University of Science and Technology.

Cells

293 T (ATAGENIX, ata-c11001) and Ls174t cells (ATCC, CL-188™) were maintained in DMEM (MACGENE, CM10013) plus 10% FBS and 1% penicillin-streptomycin. Caco2 cells

(ATCC, HTB-37) were maintained in MEM (MACGENE, CM10010) plus 10% FBS and 1% penicillin-streptomycin. 293-F cells were bought from Thermo Fisher (R79007), and were cultured in FreeStyle™ 293 Expression Medium (Thermo Fisher, 12,338–018) without antibiotics and serum. 293 F cells were maintained and amplified in a CO₂ incubator with orbital shaker platform in a condition of 37°C, 5% CO₂, 120 rpm. For the treatment of cells with recombinant Fc (purified by using 293-F cells, as described in the Materials and Methods) or ephrin-B-Fc proteins (purified by using 293-F cells, as described in the Materials and Methods), 24-well plates (CellBIND surface plate; Corning, 3337) was coated with recombinant protein at a concentration of 10 µg/ml in 1 × PBS (MACGENE, CC008) for 2 h at room temperature, followed by continue coating at 4°C overnight. Cells were plated into Fc or ephrin-B-Fc coated plates immediately after wash once with 1 × PBS.

Reagents

The antibodies of anti-MAP1LC3B (Cell Signaling Technology, 2775), anti-Flag (Cell Signaling Technology, 14,793), anti-HA (Cell Signaling Technology, 3724), anti-p-RPS6 (Cell Signaling Technology, 4857) and anti-SQSTM1 (Cell Signaling Technology, 39,749) for western blot were bought from Cell Signaling Technology. The antibodies of anti-Flag (F1804) and anti-HA (H9658) for immunoprecipitation were bought from Sigma-Aldrich. Anti-p-MTOR (AP0094) and anti-ATG16L1 (A1871) antibodies were bought from ABclonal. The antibodies of anti-HSPA5/BiP (sc-13,968), anti-EPHB2 (sc-130,068), anti-EPHB3 (sc-100,299), anti-GFP (sc-9996), anti-HSP90 (sc-13,119), anti-ACTB (sc-70,319), anti-His (sc-8036) and anti-Ub (sc-8017) antibodies were bought from Santa Cruz Biotechnology. The antibody of anti-MYC was bought from GNI (GNI4110-MC). Anti-ATG5 was from MBL life science (M153-3). Anti-EFN1/ephrin-B1 antibody was bought from Absin (abs136501). Anti-LYZ/lysozyme antibody was bought from Thermo Fisher (PA5-16,668). Anti-RNF186 antibodies for immunohistochemistry were bought from Sigma-Aldrich (HPA034547), and anti-RNF186 polyclonal antibodies for western blot was made by ATAGENIX company. E2-Ubiquitin Conjugation Kit was bought from Abcam (ab139472). DSS (molecular mass, 40,000 kilodaltons) was bought from MP Biomedicals (160,110). FreeStyle™ 293-F cells and FreeStyle™ 293 Expression Medium was bought from Thermo Fisher (R79007 and 12,338–018). FectoPRO transfection reagent was bought from Polyplus Transfection (116–001). ULK inhibitor SBI-0206965 (T2128), PtdIns3K inhibitor 3-MA (T1879), wortmannin (T6283) and Vps34-IN-1 (T7015) were bought from TargetMol.

Immunoblot and immunoprecipitation

Cells were harvested and lysed on ice in a lysis buffer containing 0.5% Triton X-100 (Solarbio, T8200), 20 mM HEPES, pH 7.4, 150 mM NaCl, 12.5 mM β-glycerophosphate (APEXBIO, 13,408–09-8), 1.5 mM MgCl₂, 10 mM NaF, 2 mM dithiothreitol, 1 mM sodium orthovanadate, 2 mM EGTA, 20 mM

aprotinin (TargetMol, C0001), 1 mM phenylmethylsulfonyl fluoride (MCE, 329–98-6) for 30 min on ice, followed by centrifuging at $13,680 \times g$ for 15 min to extract clear lysates. For immunoprecipitation, cell lysates were incubated with 1 μ g antibody at 4°C overnight, followed by incubation with A-sepharose or G-sepharose beads (Solarbio, P2040) for 4 h at 4°C, and the beads were washed four times with lysis buffer and the precipitates were eluted with 2 \times sample buffer. Elutes and whole cell extracts were resolved on SDS-PAGE followed by immunoblotting with antibodies. Densitometric quantification of western blot was performed on images of scanned films using Image J, and the bands detection was within the linear range.

Immunofluorescence

Cells were fixed with 4% paraformaldehyde and followed by permeabilization treatment with PBS containing 0.3% Triton X-100 for 10 min. Prior to incubation with primary antibody, samples were incubated with 10% goat serum at room temperature for 1 h to block nonspecific staining. After 12 h of incubation with primary antibody at 4°C, the samples were washed three times with ice cold PBS and further stained with fluorophore (Alexa Fluor 488 and Alexa Fluor 594 conjugated secondary antibodies). After staining, samples were counter stained with DAPI and immersed in mounting medium. Samples were analyzed using OLYMPUS FV3000 microscopy with companion software. Quantifications of Figure 3L–O, Figure 5E and Fig. S2B were performed as follows: the cells which contained MAP1LC3B aggregations were counted, and total of 300 cells were counted. Quantifications of Fig. S2A were performed as follows: the numbers of ATG16L1 aggregations per cells were counted, and total of 300 cells were counted.

Immunohistochemistry

Formalin-fixed and paraffin-embedded colon sections were deparaffined, rehydrated, and pretreated with 3% hydrogen peroxidase in PBS buffer for 20 min. Antigen retrieval in DAKO's antigen retrieval buffer was conducted in a steam cooker for 20 min at 96°C, followed by slowly cooling down at room temperature. After blocking with DAKO's block buffer, avidin/biotin block, sections were incubated with anti-RNF186 (1:100, HPA034547), anti-LYZ/lysozyme (1:100, PA5-16,668) overnight at 4°C. After incubation with biotin-conjugated secondary antibody and streptavidin-HRP, positive signals were visualized by DAB kit (Solarbio, DA1010) and counterstained with Harris hematoxylin (Solarbio, G1140).

For the histological scoring, slides were then examined and scored in a blinded fashion using a previously published grading system [56]. Briefly, histology was scored as follows: –Epithelium (E): 0, normal morphology; 1, loss of goblet cells; 2, loss of goblet cells in large areas; 3, loss of crypts; and 4, loss of crypts in large areas. –Infiltration (I): 0, no infiltration; 1, infiltration around crypt bases; 2, infiltration reaching the muscularis mucosa; 3, extensive infiltration reaching the muscularis mucosa and thickening of the mucosa with abundant

edema; and 4, infiltration of the submucosa. The total histological score was the sum of the epithelium and infiltration scores (total score = E + I), and thus ranged from 0 to 8.

Mass spectrometry identification

Empty vector or Flag-hRNF186 stable transfected Ls174t cells were immunoprecipitated by Flag antibody. Protein was eluted and analyzed by mass spectrometry. For the identification of EPHB2 ubiquitination sites by RNF186, 293 T cells were transfected with Flag-EPHB2 or Flag-EPHB2 together with HA-RNF186, followed by immunoprecipitation with anti-Flag antibodies. Proteins were eluted and analyzed by mass spectrometry.

Samples were reduced and alkylated in dithiothreitol (DTT) and iodoacetamide followed by trypsin digestion overnight. Digested samples were injected onto Agilent Zorbax 300SB-C18 0.075 mm x 150 mm column on Eskigent nanoLC system coupled with Thermo LTQ-ETD-Orbitrap. Advion Triversa nanomate served as the nano-ion spray source. MSMS data were searched against Refseq human protein database by Sorcerer Sequest. The searched dataset was processed by TPP (Trans-Proteomics Pipeline) and filtered with Peptide Prophet.

In vivo and in vitro ubiquitination experiment

Cells were harvested by washing with cold PBS and then were lysed with a 1% SDS solution. The lysates were then sonicated for 15 s on ice to disrupt the DNA. The lysates were boiled at 95°C for 5 min to dissociate the protein interaction. The boiled samples were diluted with co-IP buffer to 0.1% SDS and incubated on ice for 30 min, followed by centrifugation at $13,680 \times g$ for 5 min, after which the pellet was discarded. The supernatants were then incubated with protein A/G-Sepharose and antibodies against Flag, and they were rotated at 4°C overnight. The protein A/G-Sepharose beads were then pelleted and washed four times with co-IP buffer. The precipitates were resolved by SDS-PAGE and subjected to western blotting with antibodies against HA or MYC.

For His-Ub transfected ubiquitination experiments, cells were frozen in liquid nitrogen and lysed with a lysis buffer containing 8 M urea, 100 mM NaH_2PO_4 and 100 mM Tris-base, pH 8.0. The lysates were then sonicated for 15 s on ice to disrupt the DNA, followed by centrifuging at $13,680 \times g$ for 10 min to extract clear lysates. For immunoprecipitation, cell lysates were incubated with Ni-NTA at room temperature for 6 h, and the beads were washed four times with buffer containing 8 M urea, 100 mM NaH_2PO_4 and 100 mM Tris-base, pH 6.3 and the precipitates were eluted with 1 \times sample buffer. Elutes and whole cell extracts were resolved on SDS-PAGE followed by immunoblotting with antibodies. For in vitro ubiquitination experiment, experiment was performed by using E2-Ubiquitin Conjugation Kit according to manufacturer instruction. Full-length His-tagged RNF186 and EPHB2 were purified by using His-tagged protein purification kit.

Lentivirus-mediated gene knockout

pLV-U6g-EPCG and LentiCRISPR-V2 vectors were used for CRISPR-Cas9-mediated gene knockout in cell lines. Briefly,

lentivirus vector expressing g-RNA was transfected together with package vectors into 293 T cells. 48 and 72 h after transfection, virus supernatants were harvested and filtrated with 0.22 μm filter. Target cells were infected twice and were sorted by flow-cytometry-mediated cell sorting or puromycin selection. For some experiments, single cell was plated into 96-well plate for single clone. Isolated single clones were verified gene knockout by western blot or DNA sequencing. In some case, pool of GFP-sorted or puromycin-selected cells were used in the experiments.

Quantitative reverse-transcription PCR

Total RNA was extracted from spinal cord with TRIzol (Invitrogen) according to the manufacturer's instructions. 1 μg total RNA for each sample was reverse transcribed using the HiScript[®] II Q RT SuperMix (Vazyme, R223-01). The resulting complementary DNA was analyzed by quantitative reverse-transcription polymerase chain reaction (qRT-PCR) using SYBR Green qRT-PCR Master Mix (Vazyme, Q311-02). All gene expression results are expressed as arbitrary units relative to *Actb* and *GAPDH* (glyceraldehyde-3-phosphate dehydrogenase) expression.

Intracellular bacterial survival assay

We preformed this experiment according to the previous reports [57]. 2×10^5 cells were plated in 12-well plates at day 0 in growing medium. At day 1, cells were incubated overnight in DMEM. At day 2 prior to the infection, cells were rinsed once in $1 \times$ PBS and incubated for 2 h with 1 ml of DMEM medium without penicillin-streptomycin. Salmonella were cultured in LB broth at 37°C, shaking at 200 rpm overnight, then diluted 1:100 and grown until $A_{600} = 0.6$. Cells were then infected with salmonella strain (MOI = 10) and the survival of bacteria was measured by the gentamicin protection assay. After 2 h of infection, cells were incubated with gentamicin (100 mg/ml) for 1 h, 4 h and 7 h. Cells were washed with PBS and lysed with PBS containing 1% Triton X-100. The colony forming units were determined on LB agar plates and salmonella survival was analyzed. Briefly, for each condition, cells were plated in triplicate in order to calculate the ratio of intracellular bacteria over a 1 h period, and bacterial replication was expressed as the mean percentage of bacteria recovered at 4 h and 7 h post-infection relative to the number of bacteria recovered after 1 h of gentamicin treatment, defined as 100%. All infections were performed in duplicate, and each experiment was repeated at least 3 times.

Purification of Fc and ephrin-B1-Fc recombinant proteins

Extracellular part of human *EFNB1* or mouse *Efnb1* cDNA without signal peptide was constructed into pINFUSE-hIgG2-Fc2 plasmid (aa 28–237 of human EFNB1, aa 25–236 of mouse EFNB1), which express tag of human IgG2 Fc. Five to six days after transient transfection of 293 F cells by using FectoPRO transfection reagent according to manufacturer's instruction, the cell supernatant was harvested and purified by affinity chromatography with protein A in accordance with

the manufacturer's purification system. The purity of the Fc and ephrin-B1-Fc proteins was examined by 10% SDS-PAGE and Coomassie Brilliant Blue staining.

Colonic epithelial cell isolation

Mice colon was washed with cold PBS and cut longitudinally. After incubation with 0.04% sodium hypochlorite (Sigma-Aldrich, 7681–52-9) for 30 min, colon was cut into small pieces, transferred to 50 ml plastic conical centrifuge tube (Jet Biofil, CFT011500) and shaken continuously in PBS buffer with 1 mM EGTA and 1 mM EDTA at room temperature for 30 min. Colonic epithelial cell in the supernatant were collected by centrifugation at $860 \times g$. The isolated colonic cells were washed twice with $1 \times$ PBS, and were lysed with $2 \times$ loading buffer for western blot analysis. The method used here was according to the previous reports [58].

DSS-induced colitis model

Experimental colitis was induced by giving 2% (w:v) DSS (M. M. 36,000–50,000 kDa; MP Biomedicals, LLC., 160,110) in drinking water ad libitum. Mice (8 weeks) were treated for 6–8 days, and then turned to normal water. For histological, gene expression, and cytokine production studies, mice were sacrificed after DSS treatment for indicated days.

For ephrin-B1-Fc recombinant protein treatment experiment, 50 μg mouse ephrin-B1-Fc or Fc recombinant proteins in 100 μl $1 \times$ PBS were intraperitoneal injection (i.p.) injected into mice at day 0, day 2, day 4, day 6 and day 8 of DSS treatment.

Statistics

Statistical analysis was performed using GraphPad Prism, version 6.0 (Graftpad Software) Non-parametric statistics was applied to compare differences between two groups. Two-sided unpaired T test was used to derive all of the P value, except for the weight changes, which were analyzed with two-way ANOVA for multiple comparisons. Log-rank (Mantel-Cox) test was used for survival analysis. $P < 0.05$ was considered to be significant. Results are shown as mean and the error bar represents standard error of mean (S.E.M). Technical or biological replicates as indicated in the figure legend.

Disclosure statement

The authors have no financial conflicts of interest.

Funding

This investigation was supported by the independent innovation grant from Huazhong University of Science & Technology [grant 2017KFYXJJ163]; and the grant from the National Natural Science Foundation of China [grants 81871280]; and the Junior Thousand Talents Program of China [to C.H.W.].

Data availability

The datasets generated during and/or analyzed during the current study are available from the corresponding author on reasonable request.

ORCID

Chenhui Wang  <http://orcid.org/0000-0002-3186-3066>

References

- [1] Hendrickson BA, Gokhale R, Cho JH. Clinical aspects and pathophysiology of inflammatory bowel disease. *Clin Microbiol Rev.* 2002;15:79–94.
- [2] Frolkis AD, Dykeman J, Negron ME, et al. Risk of surgery for inflammatory bowel diseases has decreased over time: a systematic review and meta-analysis of population-based studies. *Gastroenterology.* 2013;145:996–1006.
- [3] Cho JH. The genetics and immunopathogenesis of inflammatory bowel disease. *Nat Rev Immunol.* 2008;8:458–466.
- [4] Ng SC, Shi HY, Hamidi N, et al. Worldwide incidence and prevalence of inflammatory bowel disease in the 21st century: a systematic review of population-based studies. *Lancet.* 2018;390:2769–2778.
- [5] Cohen LJ, Cho JH, Gevers D, et al. Genetic factors and the intestinal microbiome guide development of microbe-based therapies for inflammatory bowel diseases. *Gastroenterology.* 2019;156:2174–2189.
- [6] Munkholm P. Review article: the incidence and prevalence of colorectal cancer in inflammatory bowel disease. *Aliment Pharmacol Ther.* 2003;18(Suppl 2):1–5.
- [7] Triantafyllidis JK, Nasioulas G, Kosmidis PA. Colorectal cancer and inflammatory bowel disease: epidemiology, risk factors, mechanisms of carcinogenesis and prevention strategies. *Anticancer Res.* 2009;29:2727–2737.
- [8] Levine B, Kroemer G. Autophagy in the pathogenesis of disease. *Cell.* 2008;132:27–42.
- [9] Levine B, Mizushima N, Virgin HW. Autophagy in immunity and inflammation. *Nature.* 2011;469:323–335.
- [10] Mizushima N. Autophagy: process and function. *Genes Dev.* 2007;21:2861–2873.
- [11] Cadwell K, Liu JY, Brown SL, et al. A key role for autophagy and the autophagy gene Atg16l1 in mouse and human intestinal Paneth cells. *Nature.* 2008;456:259–263.
- [12] Homer CR, Richmond AL, Rebert NA, et al. ATG16L1 and NOD2 interact in an autophagy-dependent antibacterial pathway implicated in Crohn's disease pathogenesis. *Gastroenterology.* 2010;139:1630–41,41 e1-2.
- [13] Henckaerts L, Cleynen I, Brinar M, et al. Genetic variation in the autophagy gene ULK1 and risk of Crohn's disease. *Inflamm Bowel Dis.* 2011;17:1392–1397.
- [14] McCarroll SA, Huett A, Kuballa P, et al. Deletion polymorphism upstream of IRGM associated with altered IRGM expression and Crohn's disease. *Nat Genet.* 2008;40:1107–1112.
- [15] Parkes M, Barrett JC, Prescott NJ, et al. Sequence variants in the autophagy gene IRGM and multiple other replicating loci contribute to Crohn's disease susceptibility. *Nat Genet.* 2007;39:830–832.
- [16] Barrett JC, Hansoul S, Nicolae DL, et al. Genome-wide association defines more than 30 distinct susceptibility loci for Crohn's disease. *Nat Genet.* 2008;40:955–962.
- [17] Pasquale EB. Eph-ephrin bidirectional signaling in physiology and disease. *Cell.* 2008;133:38–52.
- [18] Pasquale EB. Eph receptors and ephrins in cancer: bidirectional signalling and beyond. *Nat Rev Cancer.* 2010;10:165–180.
- [19] Adams RH, Wilkinson GA, Weiss C, et al. Roles of ephrinB ligands and EphB receptors in cardiovascular development: demarcation of arterial/venous domains, vascular morphogenesis, and sprouting angiogenesis. *Genes Dev.* 1999;13:295–306.
- [20] Henkemeyer M, Itkis OS, Ngo M, et al. Multiple EphB receptor tyrosine kinases shape dendritic spines in the hippocampus. *J Cell Biol.* 2003;163:1313–1326.
- [21] Dalva MB, Takasu MA, Lin MZ, et al. EphB receptors interact with NMDA receptors and regulate excitatory synapse formation. *Cell.* 2000;103:945–956.
- [22] Holmberg J, Genander M, Halford MM, et al. EphB receptors coordinate migration and proliferation in the intestinal stem cell niche. *Cell.* 2006;125:1151–1163.
- [23] Batlle E, Henderson JT, Beghtel H, et al. Beta-catenin and TCF mediate cell positioning in the intestinal epithelium by controlling the expression of EphB/ephrinB. *Cell.* 2002;111:251–263.
- [24] Batlle E, Bacani J, Beghtel H, et al. EphB receptor activity suppresses colorectal cancer progression. *Nature.* 2005;435:1126–1130.
- [25] Cortina C, Palomo-Ponce S, Iglesias M, et al. EphB-ephrin-B interactions suppress colorectal cancer progression by compartmentalizing tumor cells. *Nat Genet.* 2007;39:1376–1383.
- [26] Genander M, Halford MM, Xu NJ, et al. Dissociation of EphB2 signaling pathways mediating progenitor cell proliferation and tumor suppression. *Cell.* 2009;139:679–692.
- [27] Merlos-Suarez A, Barriga FM, Jung P, et al. The intestinal stem cell signature identifies colorectal cancer stem cells and predicts disease relapse. *Cell Stem Cell.* 2011;8:511–524.
- [28] Chen J, He R, Sun W, et al. TAGAP instructs Th17 differentiation by bridging Dectin activation to EPHB2 signaling in innate antifungal response. *Nat Commun.* 2020;11:1913.
- [29] Rivas MA, Graham D, Sulem P, et al. A protein-truncating R179X variant in RNF186 confers protection against ulcerative colitis. *Nat Commun.* 2016;7:12342.
- [30] Yang SK, Hong M, Zhao W, et al. Genome-wide association study of ulcerative colitis in Koreans suggests extensive overlapping of genetic susceptibility with Caucasians. *Inflamm Bowel Dis.* 2013;19:954–966.
- [31] Beaudoin M, Goyette P, Boucher G, et al. Deep resequencing of GWAS loci identifies rare variants in CARD9, IL23R and RNF186 that are associated with ulcerative colitis. *PLoS Genet.* 2013;9:e1003723.
- [32] Fujimoto K, Kinoshita M, Tanaka H, et al. Regulation of intestinal homeostasis by the ulcerative colitis-associated gene RNF186. *Mucosal Immunol.* 2017;10:446–459.
- [33] Wang P, Wu Y, Li Y, et al. A novel RING finger E3 ligase RNF186 regulate ER stress-mediated apoptosis through interaction with BNIP1. *Cell Signal.* 2013;25:2320–2333.
- [34] Tanabe H, Kuribayashi K, Tsuji N, et al. Sesamin induces autophagy in colon cancer cells by reducing tyrosine phosphorylation of EphA1 and EphB2. *Int J Oncol.* 2011;39:33–40.
- [35] van Wijk SJ, de Vries SJ, Kemmeren P, et al. A comprehensive framework of E2-RING E3 interactions of the human ubiquitin-proteasome system. *Mol Syst Biol.* 2009;5:295.
- [36] Jung CH, Ro SH, Cao J, et al. mTOR regulation of autophagy. *FEBS Lett.* 2010;584:1287–1295.
- [37] Kim J, Kundu M, Viollet B, et al. AMPK and mTOR regulate autophagy through direct phosphorylation of Ulk1. *Nat Cell Biol.* 2011;13:132–141.
- [38] Lassen KG, McKenzie CI, Mari M, et al. Genetic Coding Variant in GPR65 Alters Lysosomal pH and Links Lysosomal Dysfunction with Colitis Risk. *Immunity.* 2016;44:1392–1405.
- [39] Roy S, Esmailniakooshkghazi A, Patnaik S, et al. Villin-1 and gelsolin regulate changes in actin dynamics that affect cell survival signaling pathways and intestinal inflammation. *Gastroenterology.* 2018;154:1405–20 e2.
- [40] Jung CH, Jun CB, Ro SH, et al. ULK-Atg13-FIP200 complexes mediate mTOR signaling to the autophagy machinery. *Mol Biol Cell.* 2009;20:1992–2003.
- [41] Din FV, Valanciute A, Houde VP, et al. Aspirin inhibits mTOR signaling, activates AMP-activated protein kinase, and induces autophagy in colorectal cancer cells. *Gastroenterology.* 2012;142:1504–15 e3.
- [42] Schiebler M, Brown K, Hegyi K, et al. Functional drug screening reveals anticonvulsants as enhancers of mTOR-independent

- autophagic killing of *Mycobacterium tuberculosis* through inositol depletion. *EMBO Mol Med*. 2015;7:127–139.
- [43] Song JX, Sun YR, Peluso I, et al. A novel curcumin analog binds to and activates TFEB in vitro and in vivo independent of MTOR inhibition. *Autophagy*. 2016;12:1372–1389.
- [44] Vucicevic L, Misirkic M, Janjetovic K, et al. Compound C induces protective autophagy in cancer cells through AMPK inhibition-independent blockade of Akt/mTOR pathway. *Autophagy*. 2011;7:40–50.
- [45] Zhang X, Chen S, Song L, et al. MTOR-independent, autophagic enhancer trehalose prolongs motor neuron survival and ameliorates the autophagic flux defect in a mouse model of amyotrophic lateral sclerosis. *Autophagy*. 2014;10:588–602.
- [46] Fritz T, Niederreiter L, Adolph T, et al. Crohn's disease: NOD2, autophagy and ER stress converge. *Gut*. 2011;60:1580–1588.
- [47] Garcia-Navas R, Munder M, Mollinedo F. Depletion of L-arginine induces autophagy as a cytoprotective response to endoplasmic reticulum stress in human T lymphocytes. *Autophagy*. 2012;8:1557–1576.
- [48] Rouschop KM, van den Beucken T, Dubois L, et al. The unfolded protein response protects human tumor cells during hypoxia through regulation of the autophagy genes MAP1LC3B and ATG5. *J Clin Invest*. 2010;120:127–141.
- [49] Sakaki K, Wu J, Kaufman RJ. Protein kinase C θ is required for autophagy in response to stress in the endoplasmic reticulum. *J Biol Chem*. 2008;283:15370–15380.
- [50] Massey DC, Bredin F, Parkes M. Use of sirolimus (rapamycin) to treat refractory Crohn's disease. *Gut*. 2008;57:1294–1296.
- [51] Mutalib M, Borrelli O, Blackstock S, et al. The use of sirolimus (rapamycin) in the management of refractory inflammatory bowel disease in children. *J Crohns Colitis*. 2014;8:1730–1734.
- [52] Reinisch W, Panes J, Lemann M, et al. A multicenter, randomized, double-blind trial of everolimus versus azathioprine and placebo to maintain steroid-induced remission in patients with moderate-to-severe active Crohn's disease. *Am J Gastroenterol*. 2008;103:2284–2292.
- [53] Hidvegi T, Ewing M, Hale P, et al. An autophagy-enhancing drug promotes degradation of mutant alpha1-antitrypsin Z and reduces hepatic fibrosis. *Science*. 2010;329:229–232.
- [54] Chukkapalli S, Amessou M, Dilly AK, et al. Role of the EphB2 receptor in autophagy, apoptosis and invasion in human breast cancer cells. *Exp Cell Res*. 2014;320:233–246.
- [55] Kandouz M, Haidara K, Zhao J, et al. The EphB2 tumor suppressor induces autophagic cell death via concomitant activation of the ERK1/2 and PI3K pathways. *Cell Cycle*. 2010;9:398–407.
- [56] Takagi T, Naito Y, Uchiyama K, et al. Carbon monoxide liberated from carbon monoxide-releasing molecule exerts an anti-inflammatory effect on dextran sulfate sodium-induced colitis in mice. *Dig Dis Sci*. 2011;56:1663–1671.
- [57] Mimouna S, Bazin M, Mograbi B, et al. HIF1A regulates xenophagic degradation of adherent and invasive *Escherichia coli* (AIEC). *Autophagy*. 2014;10:2333–2345.
- [58] Xiao H, Gulen MF, Qin J, et al. The Toll-interleukin-1 receptor member SIGIRR regulates colonic epithelial homeostasis, inflammation, and tumorigenesis. *Immunity*. 2007;26:461–475.